1-1-2020

Computational Modeling Of Shock Wave Propagation In A Layered Composites

Nicholas Ryan Scott

COMPUTATIONAL MODELING OF SHOCK WAVE PROPAGATION IN A LAYERED COMPOSITES

A Thesis
presented in partial fulfillment of requirements
for the degree of Master of Science
in the Department of Mechanical Engineering
The University of Mississippi

by

NICHOLAS R. SCOTT

May 2020

ABSTRACT

Modeling and simulation of a metallic flyer plate impacting a woven glass-fiber reinforced plastic (GRP) plate at different velocities was performed using the ALE3D© finite element code. The one-dimensional strain-based shock wave propagation experimental data in terms of time history of GRP's back surface material particle velocity, available in open literature [1], were utilized in the calibration of a continuum damage mechanics (CDM) model. The experimental data included D7 Tool Steel and 7075-T6 aluminum flyer plates and two different GRP thicknesses (6.8 mm or 13.6 mm) with varying impact velocities in the range of about 8.5 m/s to 418 m/s. For the sake of simplicity, the finite element model considered in the simulations was a planar 0/90 bidirectional plies with a thickness of 0.68 mm stacked to reach the total laminate thicknesses. The computational model used the same fiber volume fraction for the GRP target plate as in the experiments. To match measured particle velocities, the experimentally determined tetragonal symmetry stiffness matrix for the GRP and a hyperelastic continuum damage model to describe the inelastic strains were employed in ALE3D simulations. The modeling efforts also included an investigation on the influence of parameters such as impact velocities, flyer material, and GRP thickness on the free surface particle velocity histories. The damage model realistically captured several salient features of the experimental wave profiles in terms of the shock rise time and the shape of "plastic" portions beyond the Hugoniot Elastic Limit (HEL). The computational results further demonstrated the capability of a CDM based hyperelastic damage model under shear and compressive loading conditions in reproducing the inelastic portions observed in the measured particle velocity profiles.

DEDICATION

This work is dedicated to my parents, Karen and Rodney Scott. Their tireless encouragement has given me the push I needed to continue through these trying times.

LIST OF ABBREVIATIONS AND SYMBOLS

GRP Glass Reinforced Polymer

SR Strain Rate Sensitive Parameter

μm Micrometer or Micron

G Shear Modulus

K Bulk Modulus

HEL Hugoniot Elastic Limit

CDM Continuum Damage Models

ACKNOWLEDGMENTS

I would like to thank Dr. A.M. Rajendran for his consistent guidance and assistance in editing the final document. I would also like to thank Matthew Nelms for his integral support in ALE3D which allowed me to progress to this point in my studies.

TABLE OF CONTENTS

LIST OF TABLES

LIST OF FIGURES

CHAPTER I

INTRODUCTION

Dynamic response of glass fiber reinforced plastics (GRP) is complex and not fully understood. Modeling of the constitutive response of GRP type materials under high velocity impact loading conditions still remains as a great challenge. The complexity is further enhanced due to the architecture of a woven GRP. The impact response of GRP is highly nonlinear due to both geometrical and material nonlinearities. In projectile penetration into GRP panels, each of the failure mechanisms, such as fiber breakage, fiber pulling, fiber buckling, fiber sliding, inter laminar delamination, and microcracking of resin (matrix) occur in the GRP panel under multiaxial stress/strain loading conditions. An in-depth literature survey of these various processes is beyond the scope of this paper. However, there are large number of review articles available in open literature [2-5]. To fundamentally understand the damage processes and their effects on material deformation, it becomes essential to consider experimental measurements under an idealized stress/strain state, such as the plate impact test which ensures a one-dimensional strain condition. In this conventional shock wave experimental configuration, a thin metallic or plastic flyer plate (disc) impacts a stationary thick GRP target plate (disc) at high velocity. Below a certain threshold velocity (or stress) level, the target material response remains elastic. As the impact velocity increases above this threshold level, the deformation becomes "inelastic" and in addition to the elastic waves, so called "plastic" waves are generated in GRP.

During the past 4 decades, several investigators measured fundamental shock properties of all

types of materials (metals, ceramics, cement, concrete, rocks, and layered polymeric composites) using plate impact configurations. Free surface velocity measurements using the VISAR (Velocity Interferometer System of Any Reflector) on the target's back surface provide data for the loading (compression) and unloading (release) paths. Many discussions of planar impact are available in open literature and for example, Asay and Lipkin described the plate impact technique in a fundamental manner for determining dynamic yield in shocked materials [6].

In a plate impact experiment, compressive stresses are produced and transmitted immediately from the plane of impact to the adjacent stress-free areas of the material in the form of a stress pulse. When the stress pulse reaches a free surface, it reflects back as a release wave and unloads the material to a stress-free state. When two release waves interact, a triaxial tensile stress state is produced; if the tensile stress amplitudes are large enough, the material will subsequently fail. In metals, such failure occurs only when the initial shock stress exceeds the HEL; in ceramics, however, tensile failure can occur even at stress levels well below the HEL. Measurement of the free surface velocity history at the rear of the target plate provides information regarding the loading (compression) and unloading (release) paths. Since these measurements are made prior to the arrival of release waves from the lateral stress-free surfaces, the strain state remains strictly one-dimensional, while the stress state is three-dimensional.

Plate impact tests are also conducted to measure the dynamic compressive strength of the material (under one-dimensional strain) at very high strain rates [6]. The amplitude at which the elastic to plastic transition occurs is often called the HEL. In isotropic, homogeneous materials, the compressive strength can be determined from the time history of particle velocity using appropriate governing relationships [7-9]. Due to wave reflections and transmissions between all

plies in a GRP plate, the determination of compressive strength and interpretation of the wave profiles often require computational modeling. However, there are theoretical analyses [10-12] which enable the calculation of stresses in each layer based on the impedance (defined as density times the wave speed) of the layers. The observed shock structure of the experimentally measured shock wave profile (a plot of particle velocity versus time) in a GRP target plate due to a planar plate impact is often very complex and difficult to interpret in terms of precursor decay [13-15] and the shape of "inelastic" wave portion of the wave profiles.

The analysis of shock wave propagation in GRP type of heterogeneous materials with complex interfaces is very challenging. Damage initiation and growth often occur in GRP under compressive loading conditions. One of the reasons that the damage processes are poorly understood is due to our inability to recover the target under a one-dimension loading condition. Though there are recovery tests performed in metals and ceramics [16-18], it is very difficult to perform shock recovery tests on GRP. The release waves from all boundaries under a very high stress triaxialilty delaminates the GRP like a deck of cards (plies or individual fabric) during the plate impact test. The measured spall strength in GRP is very low, 7 MPa to 60 MPa [19].

The particle velocity profiles obtained for woven GRPs by Tsai, et al., at the Case Western University [1] exhibited complex elastic-plastic transitions at various shock stress levels. In their planar plate impact experiments, the flyer thickness was chosen so that release waves from the free-end of the flyer did not influence the VISAR measurements of the GRP. In their *Journal of Applied Physics* (JAP) paper [1], Tsai et al., provided plots of free surface particle velocity (VISAR) histories for 12 different plate impact tests covering two different average thicknesses (6.74 mm and 13.73 mm) of the GRP target with shock stresses ranging between 0.039 GPa to 2.6

GPa. While the use of thick high-density tool steel flyers provided data at higher shock stresses, 7075-T6 aluminum flyers yielded lower shock stresses. They derived the equation of state for the S2 glass fiber / polyester matrix composite laminate in terms of shock velocity (US) and material particle velocity (up). The analysis by Tsai et al., on shock wave propagation in GRP also included Hugoniot data at very high shock stress levels (~20 GPa) from other investigators [Dandekar et al.] to construct a complete picture on the nonlinear portion of the Hugoniot curve for GRP.

The main objective of the present work is to perform computational modeling 9 of the 12 plate impact experiments, that capture the range of material responses of the GRP, as reported in Figures 4 and 5 in the JAP article by Tsai et al. [1] towards interpreting the "inelastic" portion of the measured free surface wave particle velocity profiles (or VISAR signals). For this purpose, we used the continuum damage mechanics (CDM) based model by Barham, King, Mseis, and Faux at the Lawrence Livermore National Laboratory [20] . They utilized the Helmholtz free energy function for fiber-reinforced expression [21] to derive stress-strain relationship. This ad-hoc damage model includes a number of model constants to describe stress and stiffness degradation due to fiber breaking, fiber buckling, matrix cracking and ply delamination. We assumed that these progressive damage processes, especially under compression/shear loading conditions, generate the inelastic deformations during shock compression as observed from the VISAR signals in the plate impact experiments by Tsai et al.

The plate impact experimental configurations are described in Section 2. The experimental data form the 12 tests reported by Tsai et al., are presented with tables and figures. For the sake of completion, this section provides all necessary details of the materials and geometries related to the flyer and target plates. We briefly described the CDM damage model and its capabilities

in Section 3. The ALE3D@ finite element model [22] of the GRP and model parameters are provided in Section 4. This section presents results from a sensitivity study of a few model parameters to capture certain salient features of the free surface velocity profiles. We analyzed shock stress and damage evolutions at different locations inside the target plate including the decay of stress amplitude at the elastic-inelastic transition points. We also investigated the computationally constructed Hugoniot curve for the GRP and compared with the experimental data of Tsai et al [1]. Section 5 summarizes the results from the computational analysis of the 9 plate impact experiments.

CHAPTER II

EXPERIMENTAL SETUP

For the sake of completion, we are presenting a synopsis of the plate impact experiments of Tsai et al [1] in this section. The schematic of a typical plate impact experimental setup is shown in Figure 1. Tsai et al., used an 82.5 mm bore single stage gas gun for launching a fiberglass projectile that carries the metal flyer. The flyer was sufficiently thick to prevent release waves from the 75 mm diameter flyer plate's back and lateral surfaces from reaching the center portion of the 54 mm square target plate in the time span of VISAR measurements. Tsai et al., [1] further ensured that the lateral Rotation and tilt of the flyer plate were prevented through the use of a seal and key in the fiberglass projectile and optical alignment, ensuring a uniaxial strain conditions in their experiments. In addition, the slight amount of tilts in all tests were measured using four voltage-biased pins affixed to the target plate. The tilt data were used to correct the shock wave speed measurements in the experiments.

In plate impact experiments, a thin (60-125 nm) aluminum coating was applied to the back surface of the 54 mm square GRP plate so that the time history of particle velocity could be obtained through the use of a multibeam VALYN™ VISAR probe. In all their experiments, no transparent plastic windows were used at the back surface and all particle velocity measurements were made directly on the aluminum coated surface

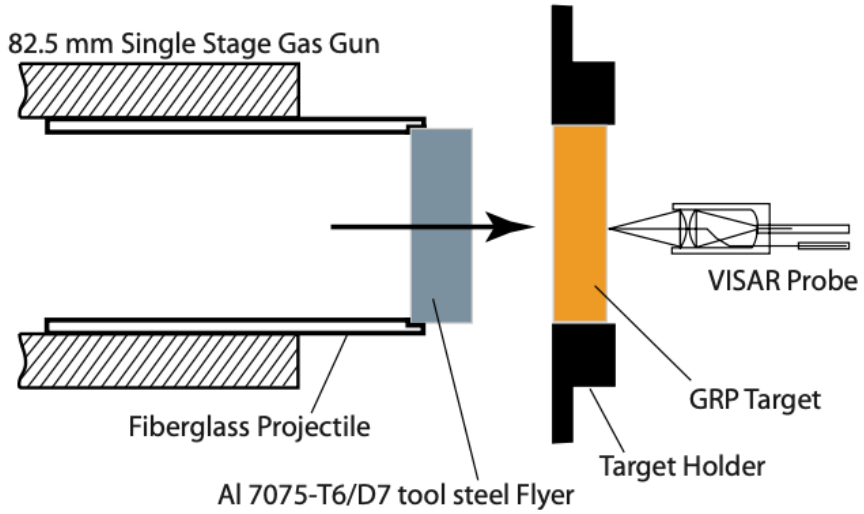

Figure 1. Plate Impact Experimental Setup Completed by Tsai et al. [1] Drawing is not to scale.

The glass fiber reinforced composite (GRP) was composed of Cycom 4102 polyester structural resin and woven 0/90 S2 glass fiber bundles. The individual ply (fabric) thickness was estimated to be 0.68 mm. Several thicknesses of GRP were used in the experiment, to measure the shock wave speed and to evaluate the effect of composite thickness to shock wave propagation, especially to observe precursor decay type phenomenon. In addition, the experimental configurations and conditions were designed in a manner to probe a variety of shock properties and parameters, such as the shock speed, Hugoniot stress and strain, elastic-plastic transition, shock rise time. Tsai et al., [1] reported 34 experiments in *Table II* of their JAP paper. Since they provided the free surface velocity history data for 12 experiments through their *Figures 4 and 5* in JAP paper, we selected representative 9 plate impact tests among them as given below in Table 1.

Table 1. Selected tests for ALE3D simulations and modeling

Test #	Flyer	Target Thickness (mm)	Impact Velocity (m/sec)
LT 25	Al 7075-T6	6.8	184.29
LT 30	Al 7075-T6	6.8	111.69
LT 31	Al 7075-T6	6.8	312.7
LT 38	Al 7075-T6	13.6	8.5
LT 40	Al 7075-T6	13.6	108.1
LT 44	Al 7075-T6	13.6	68.69
LT 47	D7 Tool Steel	6.8	367.88
LT 48	D7 Tool Steel	6.8	417.96
LT 51	Al 7075-T6	13.6	172.76

For instance, a careful examination of this table showed that LT 30 and LT 40 were at approximately same impact velocity levels for the thin and thick GRP, respectively. The VISAR profiles provide some insight into the deformation processes in the GRP both under elastic and inelastic strain conditions. It is reasonable to expect that a comparison analysis of these two experiments through a detailed computational modeling may reveal how the shock front structure evolves as it propagates farther distance from the impact plane while matching the VISAR data with results from the ALE3D code.

Figure 2, shows data for a number of test configurations with a range of impact velocities and different flyer materials and target thicknesses. For the purpose of modeling, we selected LT 25, LT 30, LT 31, LT 40, LT 47, and LT 48 from among all test data shown. The first set of plots in Figure 2a is for a thinner target thickness (6.5 mm to 6.88 mm) while Figure 2b is for larger thickness of 12.99 mm to 13.59 mm.

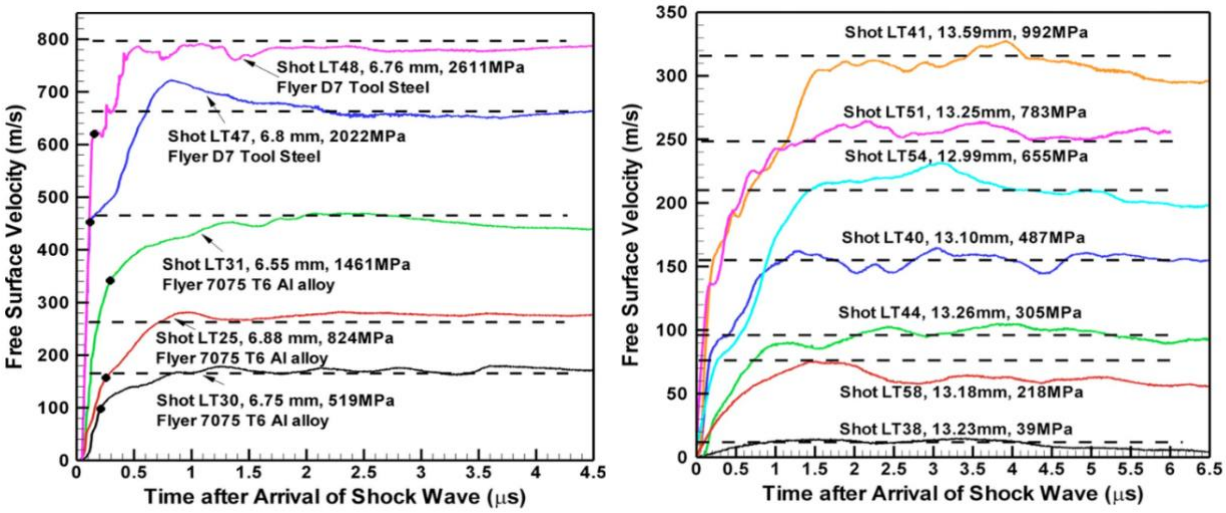

(a) (b)

Figure 2. Experimentally determined free surface particle velocity versus time for GRP thickness of ~7mm (a) and ~13mm (b) [1]

Tsai et al., [1] analyzed the free surface particle velocity profiles to derive certain conclusions on the shock wave propagation characteristics in GRP. The black circular markers on the profiles in Figure 2a are the transition points at which certain nonlinear response occurs due to the viscoelastic response of polymeric materials in GRP. They also speculate that these HEL looking points are not the same as seen in the elastic-plastic transition points in VISAR signals for metallic materials or crystalline ceramics. More in-depth discussions on these wave profiles can be found in reference in their JAP article [1].

The salient features in the free surface velocity profiles (signals) are: the rise time, elastic (linear) to inelastic (nonlinear) transition points, the shape of the nonlinear portion of the rising signals, the peak velocity amplitudes, and the observed late time oscillations of the particle velocity. In Figure 2b, the oscillations in LT 40 beyond 1.5 microseconds is due to complex wave reflections, attenuations, and dispersions in GRP due to material heterogeneities, such as

the interfaces between plies, and interfaces between glass fiber and resin, and other geometrical heterogeneities. The oscillations are more enhanced in thick composites due to longer wave propagation distances from the impact plane as can be seen in several other profiles in Figure 2b. We can also observe from these profiles that the rise time (the time it takes for the velocity to reach the peak) increases with increasing impact velocities. The velocity profiles become much steeper at high shock stress levels approximately above 1.5 GPa as compared with low shock stress levels. It is important to note that since the stress histories inside the GRP targets are not measured in the experiments using any stress gauges [13,23], the shock stresses are calculated using the Rankine-Hugoniot conservation equations [24,25]. The corresponding equation for the Hugoniot stress is,

Equation 1 $$\boldsymbol{\sigma_H} = \frac{\boldsymbol{\rho_0 C_0^2 \varepsilon_H}}{\boldsymbol{(1-S\varepsilon_H)}}$$

Where, ρ_0 is the initial density, C_0 is sound speed, ε_H is Hugoniot strain (volumetric strain), and S is a parameter. This empirical parameter, S is often determined from shock propagation experiments.

The stiffness matrix of the S2 glass fiber woven composite was found through a series of experiments performed by Tsai et al [1]. In Table 2, the elastic constants are supplied in the form that the composite strength model in ALE3D requires. The longitudinal wave speed will be referred to several times to verify the different formulations of the material deck. Both E_a and E_b are the same, similar to G_{bc} and G_{ca}, given the fact that the fibers are in the a and b direction 0_0 / 90_0. The a-direction will be the y-direction, while the b-direction will be the z-direction. Since

the shock wave is perpendicular to the 0/90 fiber orientation, it is propagating in the x direction. Given that the wave front is propagating primarily through the matrix, a secondary objective of this thesis is to see whether the matrix and fibers contribute equally to the wave speed, and therefore require a full description of the GRP for damage, or whether the wave speed is primarily dependent on the matrix, and only requires the matrix description for damage.

Table 2. Elastic Constants of the Woven GRP Found in Experiments by Tsai et al. [1]

Density (g/cm^3)	E_a (GPa)	E_b (GPa)	E_c (GPa)	υ_{ba}	υ_{ca}	υ_{cb}	G_{ab} (GPa)	G_{bc} (GPa)	G_{ca} (GPa)	Longitudinal Wave Speed (km/s)	Bulk Wave Speed (km/s)
1.959	22.203	22.203	16.11	0.4151	0.2057	0.2057	4.9407	4.63	4.63	3.2	2.6

Computational modeling of these experiments with realistic constitutive/damage evolution equations and equation states of the GRP constituents often provides some insights into the wave propagation in the target. The foot prints of all wave reflections and dispersions, and damage nucleation and evolution under shock compression are captured in the measured data of free surface velocity profiles. It is possible to derive certain conclusions on wave propagation characteristics based on the model's ability to match the computational model generated profiles with the data.

CHAPTER III

COMPUTATIONAL METHOD

III.1 Computational Model

The Arbitrary Lagrangian-Eulerian three-dimensional (ALE3D) Code [22] developed at the Lawrence Livermore National Laboratory (LLNL) was employed in the simulations of plate impact experiments listed in Table 1. The individual ply thickness of the GRP was approximately 0.68 mm, so 10 plies were used to create the ~7mm thick composite, and 20 plies were used for the ~13mm GRP. Each ply is considered perfectly bonded to its neighboring ply to create the overall 6.8x0.17x0.17 mm representative area of the composite, and is composed of 25 elements. Since we employed a computational continuum modeling approach, the ply interfaces are not explicitly modeled through any cohesive type model.

Table 3 provides some details of the computational model for both flyer and target. The size (height) of the elements in the shockwave direction are roughly equal (0.17 mm) for both flyer and target. The mesh design is such that the target and flyer faces contacted exactly node to node, which assured robust contact response. Each ply has the same number of elements, and the length of the element is approximately 27.2 micrometers.

Table 3. Computational Mesh Description for the Thin (~7 mm) GRP and 25 mm thick Flyer

Total Elements	Total Nodes	Flyer Height (mm)	Flyer Length (mm)	Flyer Elements	Target Height (mm)	Target Length (mm)	Target Elements
125000	151492	0.17	25	100000	0.17	6.8	25000

Using appropriate periodic boundary conditions (BC) on all lateral boundaries, the simulations were performed to ensure one dimensional strain state by preventing displacement in the y and z directions and by allowing particle motion only in the x direction. This BC prevents lateral release waves from occurring for the full duration of the solution which is approximately 9 microseconds for the thick (13 mm) composite. A very thick (25 mm) flyer was modeled so that the release waves from the stress-free back surface of the flyer would not transmit into the 7 mm or 13 mm thick GRP target plates at least up to 10 microseconds of solution duration. This flyer thickness was held consistent through all simulations.

A portion of the 3D interior section of the flyer and GRP is modeled to ensure computational tractability using parallelepiped elements of 27.2 microns thick. The small section as shown in Figure 3 was determined to be free of lateral waves over the period of time of interest became the dimensions of the computational flyer and GRP in all simulations. The ALE3D computational models were developed for a 7 mm (thin) GRP and 13 mm (thick) GRP, respectively and for two different 25 mm thick flyers, 7075-T6 aluminum and tool steel, respectively. To develop a fundamental understanding of the shock wave response of GRP, a comparison study between the VISAR data and results from the plate impact simulations was performed for the 9 tests at various impact velocities as listed in Table 1.

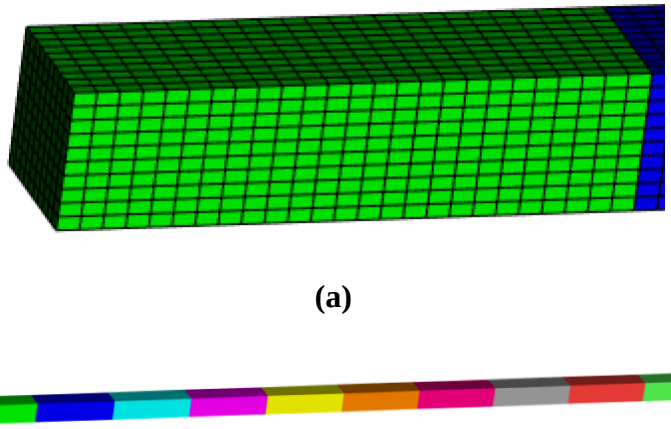

(a)

(b)

Figure 3. Schematic of ALE3D Meshed GRP using VISIT post-processor. (a) the enlarged view of the first ply, showing the detailed mesh. (b) the full GRP model, each color signifies the individual ply (10 plies for the thin GRP target and 20 plies for the thick GRP)

III.2 Constitutive Model

For the aluminum and steel flyers, strain rate dependent Steinberg-Lund (S-L) material model [23] that is available in the ALE3D code were employed. Since the response of flyer materials remains elastic-plastic without any damage or failure under the impact velocities considered in the simulations, there is no need for a damage model. However, the GRP was characterized by a damage dependent strength and yield surface models. In order to study the non-linear response of the GRP under higher velocity impact, the GRP was considered as an anisotropic hyperelastic material with various types of progressive damage. This strength model was specifically suitable for fiber/matrix composite materials and was modeled in such a way that each ply was 0^0 / 90^0 bidirectional. Therefore, no individual plies of 0^0 / 90^0 were explicitly modeled. While this computational description may not capture all mechanics of a 0^0 / 90^0 woven composite, however, by modeling the same fiber volume content and fiber material

properties, this approximation seems to provide realistic results.

While the strain rate dependent strength models for the metallic flyers were described by S-L model, the strength and hyperelastic constitutive models for GRP were described by the LLNL models in ALE3D. For the sake of completeness, the Steinberg and Lund model for the flyer materials (aluminum or steel) is described below. In the S-L model, the strength of the metal is expressed by,

Equation 2 $$\boldsymbol{Y} = \left[\boldsymbol{Y_T}(\dot{\boldsymbol{\varepsilon}}_{\boldsymbol{p}}, \mathbf{T}) + \boldsymbol{Y_A}(\boldsymbol{\varepsilon_p}) \right] \left[\frac{\boldsymbol{G}\,(\boldsymbol{P},\boldsymbol{T})}{\boldsymbol{G_0}} \right]$$

Where,

Equation 3 $$\dot{\boldsymbol{\varepsilon}}_{\boldsymbol{p}} = \left\{ \frac{\mathbf{1}}{\boldsymbol{C_1}} \mathbf{exp} \left[\boldsymbol{C_3} \left(\mathbf{1} - \frac{\boldsymbol{Y_T}}{\boldsymbol{C_4}} \right)^{\mathbf{2}} \right] + \frac{\boldsymbol{C_2}}{\boldsymbol{Y_T}} \right\}$$

The strength Y_T is due to thermally activated part which is a function of applied strain rate and temperature, and Y_A is the athermal part due to strain hardening. The S-L While G_0 is the initial shear modulus of the undeformed solid in room temperature, the shear modulus G varies with pressure and temperature under dynamic loading conditions. The constants $C_1, C_2, C_3$and C_4 are model parameters that can be estimated and calibrated from microstructural relationships and experiments, respectively.

The GRP constitutive equations allow for two different types of fibers, such as E2 glass, S2 glass, or Kevlar, in the composite at user specified angles or directions, and consider damage in individual fibers. Since different fiber interactions in GRP influence the strength and failure processes, the models has additional terms to describe the effects of two different fibers on the

GRP behaviors. However the current modeling involves only one type of fiber (S2 glass), therefore, both fiber groups 1 and 2 are modeled as S2 Glass, with material properties found from the Axom website's S-glass fiber page [23].

The standard hyperelastic material such as a Neo Hookean material, using an Ogden parameter of 1, or a Mooney-Rivlin material, using an Ogden parameter of 2 are typically suitable for nonlinear elastic solids, like rubber, soft tissues, and foams. We, however, employed the hyperelastic formulation with Ogden parameter value of "-2" for modeling the non-linear response of S2 glass fibers / polymeric matrix system under high velocity impact loading conditions. The model's damage parameters were calibrated using the VISAR data from Tsai et al [1]. Since the shock stress levels in the experiments are almost linear, the equation of state is integrally obtained from the hyperelastic constitutive relationships. However, modeling of VISAR data obtained by Dandekar et al., [15] at very high shock stress levels (~20 GPa) will require Mie-Gruneisen type nonlinear description for the equation of state. The shock stress level in Tsai et al [1] plate impact experiments are at shock stress levels below 3 GPa.

III.2.1 Strength Model

ALE3D uses various models to help describe a material's response while at certain stress-strain state. When the material is in the elastic portion of the stress strain curve, ALE3D uses the strength model, referred also as the elasmodel. The strength model determines how stiff the material is as well as the poisson's ratio of the material. Given that this is a woven composite approximation, the stiffnesses in the 1 and 2 direction will be equivalent. When the material yields by surpassing its elastic strength or strain, ALE3D will this use the yield surface model,

also referred to as the ysmodel. A yield surface model determines when damage initiates, how the damage evolves, and which stiffnesses to degrade based on the type of damage incurred.

This strength model was designed to be used in tangent to a composite ysmodel, and therefore the constitutive equations are defined in the ysmodel, given how different damage formulations would affect the stress strain relationships. The Fiber Composite strength model describes the overall composite anisotropy with different Young's moduli, shear moduli, Poisson's ratios as provided in Table 2. Elastic Constants of the Woven GRP Found in Experiments by Tsai et al. [1]. Since the strength (or stress) of GRP is essentially obtained from the elastic stiffness matrix, there is no strain rate dependency in the stress – strain relationship. However, the inelastic strains due to any damage initiation and accumulation under shock loading above certain shock stress level are calculated using the so called "Yield Surface" model in ALE3D. The strain rate dependency on the stress softening due to damage is introduced through damage parameters that appear in the hyperelastic CDM equations.

III.2.2 Yield Surface Model

The yield surface model for GRP in ALE3D, created by Mike King and Matt Barham, is derived from a Helmholtz Free Energy (HFE) function for cross fiber composites. An expression for the energy function can be found in the book: Nonlinear Solid Mechanics: A Continuum Approach for Engineering," by Holzapfel [21]. This yield surface model is a hyperelastic composite model that accounts for energy partitions in different fiber orientations and isotropic matrix material. The HFE function, $\boldsymbol{\psi}$ is given by,

Equation 4 $$\boldsymbol{\psi = \frac{G}{2}(\bar{I}_1 - 3) + \frac{K}{\beta^2}\left(\beta \ln J + J^{-\beta} - 1\right)I + \frac{k_1}{2}(I_4 - 1)^2 + \frac{k_2}{2}(I_6 - 1)^2}$$

While the $\bar{I}_1 = I_1 J^{-2/3}$ is the volume preserving part of the first invariant, $I_1 = tr\, C$, and I_2 is the second invariants in terms of right Cauchy-Green tensor for any isotropic material, such as the polyester or epoxy matrix, I_3, and I_4 are specially described for multidirectional fiber systems to capture fiber deformations under tension and compression. The constitutive equations derived from tis HFE function explicitly involve the fiber orientation for two types of fiber systems. The ψ function is expressed in terms of the deformation gradient and the Cauchy left tensor. The J is the Jacobian of the deformation gradient, the k1 and k2 are the modulus of the fibers, which for this paper's intent are equivalent. β is the Ogden parameter. The m_i, and m_{si} where i=1,2 are the directions of the two-fiber system. Since the GRP considered in the present study is consisting of only one fiber system, the cross terms between the two different system k_s terms in Equation 5 drops out from the equation. The stress-strain relationship, as given in Equation 5, is derived by differentiating the HFE function, ψ with respect to the strains, B_{ij},

Equation 5 $$\boldsymbol{\sigma = \frac{G}{J}\left(\bar{B} - \frac{tr(\bar{B})}{3}I\right) + \frac{K}{J\beta}\left(1 - J^{-\beta}\right)I + \frac{k_1}{J}(m_1.m_1 - 1)m_1 \otimes m_1 + \frac{k_2}{J}(m_2.m_2 - 1)m_2 \otimes m_2 + \frac{k_s}{2}(m_{s1}.m_{s1} - 1)m_{s1} \otimes m_{s1} + \frac{k_s}{2}(m_{s2}.m_{s2} - 1)m_{s2} \otimes m_{s2}}$$

The first term with the shear modulus, G in the right side of the equation is due to deviatoric (or shear) part of the deformation gradient tensor, the second term with the bulk

modulus K, is the volumetric part of the deformation gradient, and the other terms describe the stretch strains in the directions of the fiber systems.

The LLNL model introduced damage variables into the stress-strain relationship following the continuum damage mechanics approach as shown in Equation 6.

Equation 6 $$\boldsymbol{\sigma(F) = (1 - d^M)\frac{G}{J}\left(\overline{B} - \frac{tr(\overline{B})}{3} I\right) + (1 - d^M)\frac{K}{J\beta}\left(1 - J^{-\beta}\right) + d^M \frac{K^D}{v\beta}\left(1 - v^{\beta}\right) + (1 - d^{F1})\frac{k_1}{J}(m_1 . m_1 - 1)m_1 \otimes m_1 + (1 - d^{F2})\frac{k_2}{J}(m_2 . m_2 - 1)m_2 \otimes m_2 + (1 - d^{Fs})\frac{k_s}{2}(m_{s1} . m_{s1} - 1)m_{s1} \otimes m_{s1} + (1 - d^{Fs})\frac{k_s}{2}(m_{s2} . m_{s2} - 1)m_{s2} \otimes m_{s2}}$$

Note that the terms "$(\boldsymbol{m_1 . m_1 - 1})$ *and* $(\boldsymbol{m_2 . m_2 - 1})$" represent the fiber strains in direction 1 and 2, respectively. When any of the damage criterion is met (R=>1), damage begins to accumulate exponentially as seen in Equation 7. The stiffness degradation is described through the terms "(1- d)". For instance, the damaged matrix shear modulus, say G_{eff} , is defined by, $G_{eff} = (\boldsymbol{1 - d^M})G$, where G is the intact shear modulus of the matrix material. The damage parameter "d" is can be defined for different failure modes. Here, the model parameter $\boldsymbol{d^M}$ describes the matrix damage. In general, it is assumed that the damage growth under all modes follows Equation 7.

Equation 7 $$\boldsymbol{d = \begin{cases} 0 & if\ R<1 \\ 1 - exp\left(\frac{-(R-1)}{\iota}\right) & if\ R \geq 1 \end{cases}}$$

The "ι" controls the slope of the softening portion of the stress-strain curve. The exponential nature of this law controls the unloading rate of the stress when damage initiates under different modes. For instance, when the unloading modulus (E_f) is about 10 times the Elastic (or Young's Modulus), the value of ι is approximately less than 0.1. The damage, d reaches instantaneously the value of 1 indicating abrupt fracture rather than progressive.

Using this exponential damage growth model, different "R" parameters are defined for each one of the failure modes. There are 5 failure modes: Fiber breakage in tension (R_{FiT}), fiber buckling in compression (R_{FiC}), matrix cracking under shear (R_{MS}), matrix cracking under tension (R_{ME}), and delamination of the fibers (R_D). Each of these 5 "R" parameters are defined through Equation 8-12. Note that R_{FiT} and R_{FiC}, where i=1,2 are for two different fiber systems. The failure criterion states that only when the "R" value is below 1, damage initiation occurs. In other words, when the applied strain either under tension or compression loading exceeds a maximum or critical value, the "R" becomes greater than 1.

Equation 8
$$\boldsymbol{R^{FiT}} = \frac{\boldsymbol{\varepsilon^{i}}}{\boldsymbol{\varepsilon^{FiT}}}$$

ε^{FiT} is the maximum strain which is experimentally measureable and at which the stress softening begins or in other words some damage process initiates. ε^{i} is the applied strain due to dynamic loading. When the applied fiber strain (ε^{i}) is positive (> 0), the damage is described by the R_{FiT} parameter and when it is negative (< 0), the R_{FiC} models the damage process under compression. The maximum strain can be obtained from the ratio of the maximum stress (or

fiber strength) and fiber's Young's modulus. These material properties are available from the manufacture of the S-Glass fiber [23].

When the fiber bundle is under compression, two types of damage modes can be modeled using the R_{FiC} parameter: fiber buckling and fiber debonding. Equation 9 defines this parameter as the ratio of applied fiber compressive strain and critical strain at damage initiation.

Equation 9

$$\boldsymbol{R^{FiC}} = \begin{cases} \frac{\boldsymbol{\varepsilon^{i}}}{\boldsymbol{\varepsilon^{FiC}}} & \boldsymbol{damage\ in\ compression} \\ \mathbf{0} & \boldsymbol{buckle\ in\ compression} \end{cases}$$

In the current work, the GRP is allowed to experience only compressive loadings in all three directions due to the stress/strain state in a plate impact experiment prior to the arrival of any release waves from the lateral boundaries or from the back of both the flyer and target plates. When compressive damage to the fibers was included through Equation 9 in the ALE3D simulations, insignificant amount of damage occurred for the set of model constants that matched the VISAR data. For computational efficiency and model simplicity, the fiber bucking and fiber debonding types of failure modes are not modeled.

R_{MS} and R_{ME} seen in Equation 10 and Equation 11 captures the matrix based damage modes that degrade the shear and bulk moduli, respectively.

Equation 10

$$\boldsymbol{R^{MS}} = \frac{\boldsymbol{\varepsilon^{VM}}}{\boldsymbol{\varepsilon^{MS}}}$$

ε^{VM} is the von Misses strain (or effective strain) and ε^{MS} is the critical shear strain to

failure. The bulk damage criterion is defined by Equation 11, where J_{ME} is the matrix relative volume of expansion to damage. This is a user-controlled parameter that helps defining how the bulk modulus degrades.

Equation 11 $$\boldsymbol{R^{ME}} = \frac{\boldsymbol{J-1}}{\boldsymbol{J^{ME}-1}}$$

The "R" parameter R_D in Equation 12 models the ply delamination and it depends on through thickness lamina stress and shear associated with through thickness lamina and fiber directions. Tsai-Hill criterion [24] is applied at a lamina level, and it describes a smooth elliptical failure envelope. The delamination criterion is given by,

Equation 12 $$\boldsymbol{R^{D}} = \frac{\tilde{\sigma}_{33}^{2}}{(t^{D})^{2}} + \frac{\tilde{\sigma}_{13}^{2}+\tilde{\sigma}_{23}^{2}}{(s^{D})^{2}}$$

Where the 33 direction is through the thickness of the GRP, perpendicular to the 1 and 2 directions that the fibers are oriented along.

Since most fiber reinforced plastics (composites) (FRP) seemed to exhibit strain rate dependent behaviors [25], it is important to introduce a parameter that models the effects on the damage processes. In the LLNL hyperelastic damage model, it is possible to introduce strain rate dependency into any or all model parameters that are involved in equations 8 – 12. The simplest modeling approach is through the following empirical expression,

Equation 13 $$\boldsymbol{var_{current} = var(1 + c_1\, ln\left(\frac{\dot{\varepsilon}}{\dot{\varepsilon}_0}\right))}$$

Equation 13 enables the damage model to capture any viscous effects associated with the damage processes in an arbitrary manner. Further discussions of strain rate dependent response of GRP target under shock wave loading is reported in the following Section 4.

CHAPTER IV

COMPUTATIONAL RESULTS AND DISCUSSIONS

Two questions should be answered by this paper: (1) can a bidirectional homogenized anisotropic composite model predict a woven composite's response to dynamic shock loading conditions by employing properties of the woven composites, and if so, (2) what is the evolution of damage in a GRP with shock loading conditions look like? The relevance of the analysis of the second question hinges on the success of the first question. In order to predict a woven composite's behavior, a parametric study must be completed to ensure a physical and accurate explanation for the progression of damage. Then, the simulated velocity profiles and shock stresses of various impact velocities will be compared to the experimental results to determine whether the bidirectional model can predict the woven composite's material response to shock loading.

A sensitivity study was performed to see the interaction between various model parameters to allow for a better understanding beyond what the constitutive equations reveal. The damage initiation and growth as the shock wave propagates into the GRP target plate under multiaxial compressive loading greatly influence the free surface velocity (VISAR Signal), especially the non-linear portion observed in the velocity profile. The parameters considered for this purpose are: the shear modulus, shear strength, and bulk modulus of the polyester matrix, maximum damage threshold before ultimate failure, and the initial tangent modulus once

incipient damage occurs. Since the GRP considered in the present study used only one fiber system (S2 glass), the terms due to the second fiber system drops out from the constitutive equation 6. The S2 glass fibers material properties were found on Axom's website, and the lower end of the strengths were used to give a conservative estimate on how damage evolved [23]. A full list of variables the model used is in Appendix A.

IV.1 Parametric Study

All of the parameters shown below, aside from the mesh resolution, belong to the Hyperelastic Progressive Damage YS Model (see Equation 6). The influence of parameters on the free surface velocity history that pertain to how matrix and delamination damage evolve in the GRP are studied. The matrix strength was calibrated to obtain damage initiation that correlates with the initiation of non-linear region in the VISAR measured free end velocity profile. Since the experimentally determined elastic tensor for the S2 glass woven GRP laminate as given in Table 2 was used to describe the anisotropic elastic deformation, the parametric sensitivity study does not include the elastic constants, the stiffness and Poisson ratio.

IV.1.1 Mesh Resolution

Mesh dependency is inherent to damage models; true convergence will not exist due to the nature of these models without correction factors. Murakami and Liu discuss reasons for mesh-dependency in continuum damage models (CDM), and the inaccuracies of a few solutions provided to get rid of mesh dependencies [26]. One of the main ways to prevent mesh dependencies discussed in their publication, was to have mesh-dependent material properties.

This solution is not of interest for this study, as the desire for true physically determined material properties were considered important to capture that effectiveness of the model's ability to predict the GRP behavior. Ljustina et al. furthered this discussion of mesh dependency in CDM, claiming that failure models are a way to overcome mesh dependency [27]. Their findings showed, however, decoupling the stress state and the damage could not prevent inherent mesh dependencies that a conventional CDM model carries. Our study found that capturing the non-linearities for the free surface velocity required a progressive damage model, a failure model as Ljustina et al. proposed, could not provide an accurate prediction of the VISAR response. The reason for mesh dependency existing in the current study, is the softening of stiffness due to damage of a given element size. If a ply is 0.68 mm thick, and has two elements through thickness, when one of the elements is damaged ½ of the ply, or 1/20th of the full GRP, has a degradation in stiffness instantaneously. If the scenario then changes to 20 elements through the thickness and one element degrades, 1/20th of the ply, or 1/200th of the full GRP, observes a shear or bulk modulus degradation. When looking at the physical representation of the GRP, the fiber bundles are the total thickness of each ply, 0.68 mm. If a fiber begins to fail, or the whole fiber bundle fails, the stiffness of the overall ply will instantaneously deteriorate. Therefore, an infinitesimally small mesh, while being the best approximation for a strength model, would not capture the true behavior of the ply. Instead, over-discretization could cause artificial stiffnesses to occur when comparing it to the true material, due to how large of an area cracking or fiber breakage could affect. If the discretization is too small, the full true physical area that damage would be seen would span across too many elements, and may not be captured by the model.

For the purposes of modeling the continuum, a mesh was chosen so that the physical

dimensions would be able to contain a portion of the fiber bundles. The study also revealed that further discretization caused numerical instabilities, such as heavy mesh distortion and rectangular meshes inverting to create negative volume, that could only be resolved through the use of artificial viscosity. To minimize the effects of mesh size and design on the computational results, 14 different sizes and designs were considered. The size of finest meshes was a fraction of the fiber bundle size. Further resolution (less than 0.01 mm) caused numerical instabilities, such as heavy mesh distortion and rectangular meshes inverting to create negative volume, that could only be resolved through the use of artificial viscosity and other type of numerical algorithms such as remeshing, particle conversion etc. Base on the mesh sensitivity study, the resulting mesh was a rectangular mesh with an aspect ratio of 8 (thickness direction, *27.2 micron*) : 5 (fiber direction, *17.0 micron*), allowing for substantial reduction in the shock direction to handle large compressive strains. As the compressive strain increased at high velocity impact, the shape of the elements tend to become cubic with 1:1 aspect ratio approximately. Figure 4 is a mesh resolution plot of the free surface velocity that shows no convergence for the LT-30 case at 111.69 m/s for the thin composite. Uniform and non-uniform meshes between the flyer and GRP also were investigated. Since the thickness of the flyer is approximately 5 times that of the GRP, uniform mesh size across flyer and target would increase the computational time exponentially. Results from various simulations also indicated that to guarantee increased level of accuracy without any numerical instabilities, it is essential that the nodes at the contact surfaces for flyer and target make direct contact (node by node match up) based on the contact algorithm selected from ALE3D input options.

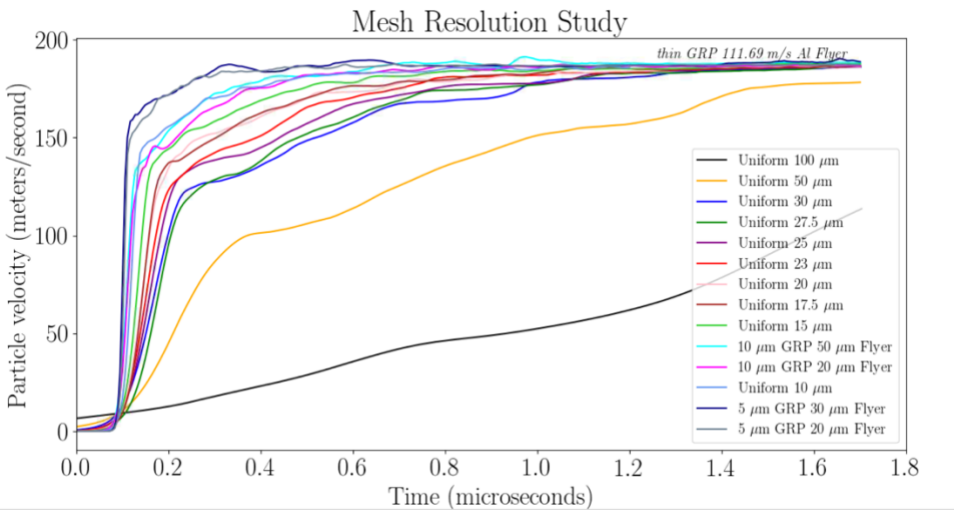

Figure 4. Mesh Convergence study for LT 30 case, at 111.69 m/s for the thin composite (6.8 mm). The chosen mesh was approximately 0.0272 mm, or 27.2 microns in the shock direction with an aspect ratio of 8:5 in shock direction vs fiber direction of the sample.

As the mesh size starts reaching nanometer scales, the slope of the elastic portion of the free surface velocity profile becomes very steep. It should also be realized that when the size becomes less than 100 nanometers, the atomistic forces become more and more important and the solutions will require molecular dynamics based computational efforts with realistic force fields for a complex material system. The comparisons between various mesh sizes further revealed that relatively a coarser mesh (27 micron) could match the VISAR measurement for the LT30 plate impact test. Since the coarser mesh is computationally efficient while the solutions realistically predicted the elastic slope of the free surface velocity profiles, all simulations in the sensitivity analysis were performed with a mesh size of 27 microns.

IV.1.2 Shear Modulus of the Matrix

Due to the fact that the shear modulus plays a significant role in shock speed, adjusting

the shear modulus (G) of the matrix causes a change in the arrival time of the shockwave in the composite. It is fairly well known that rocks, ceramics and cementitious materials like brittle solids exhibit share modulus / shear strength dependent damage evolution under multiaxial loading conditions. In Figure 5a shows damage evolutions in two different locations (1/5th and 4/5th of the thickness of the GRP away from the impact plane) along the shock wave propagation direction for two values of the shear modulus: 2, and 5 GPa, respectively.

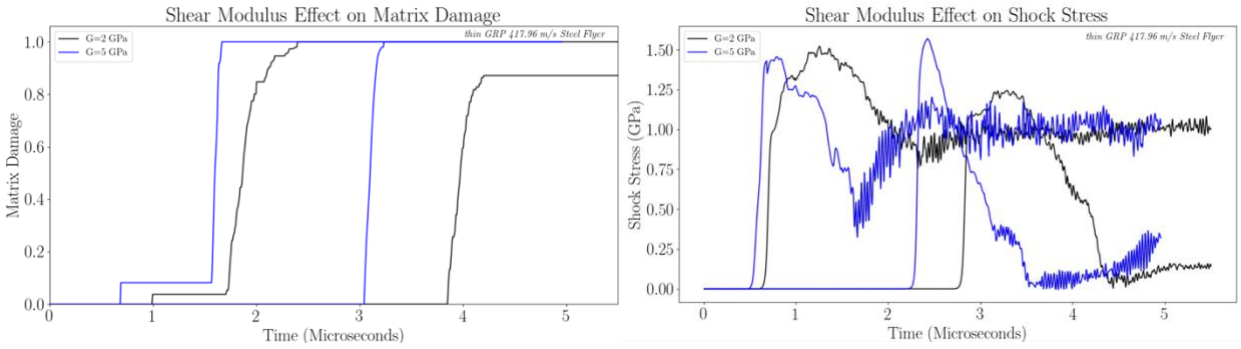

(a) (b)

Figure 5. Shear Modulus' Effect on GRP Matrix Damage Evolution (a) and Shock Stress (b). The two lines for each color are two separate locations at 1/5th and 4/5th through the thickness of the GRP.

A lower G will stave off the two matrix-based damages due to how the constitutive model's strain-based formulation, depicted in Figure 5a in the orange and blue lines. A lower G with a particular strength parameter allows for a larger amount of ductility before failure than a higher G. Hence, the hyperelastic strain relation to damage allowing for a greater level of stress before damage initiation and absolute failure of the given criterion, whether it be intra-ply delamination or matrix cracking. Figure 5b outlines that the shear modulus in the ysmodel has an affect on wave speed and shock height (seen more clearly in the 4/5th through thickness line for both colors).

In a simplified 1-D case, where $\sigma = E * \varepsilon$, if the strain of the GRP is compared for two separate cases, where one has a high and the other has low G and K moduli, but the σ is constant at a certain shock velocity due to stress equilibrium governed by Equation 14,

Equation 14 $$\sigma = \frac{1}{2}\rho\, c\, v$$

Where: ρ is the density of the flyer, c is the shock velocity, and v is the impact velocity.

then the two would have different strains. Specifically, the strain corresponding to the smaller E will be larger. If the timescale at which shock stress increases is the exact same for both scenarios, you will have a higher strain rate for the low stiffness case. This will increase the strength of the GRP, matrix, and fibers, which will make the damage criteria seen in Equation 8-12 much harder to achieve. This may be the explanation as to why the blue line in this figure shows around 90% failure or less while the orange shows complete failure for two of the three locations. Figure 6 will reinforce these findings by showing a general increase without strain rate effects.

Both Figure 5a and b show that these input parameters of the ysmodel affect the wave speed of the material, despite that traditionally belonging to the strength model. This must be accounted for to ensure proper shock velocity for the given impact velocity. Without the proper shock velocity, incorrect stresses will be calculated by the FEA code which may give an inaccurate picture to how damage evolution occurred in the experiment.

IV.1.3 Matrix Shear Strength

The matrix shear strength's effect on matrix damage showed that as strength goes up, so too does ductility, and the damage seen in the matrix decreases. Figure 6 shows a general case of the matrix damage trend, where the strain rate effects should be consistent throughout the three cases (neither G nor K are changed, so the rate at which the GRP strains should be consistent). This simplified scenario that shows as strength increases, matrix damage decreases, sheds light onto the comment stated previously. Since matrix shear strength is a strain rate sensitive variable, if a scenario increases the rate at which the target is strained, matrix damage may be delayed and the maximum damage at a location may be reduced, as seen below by comparing the black lines to the orange lines at the three separate locations.

While the arrival time of the shock doesn't change with a variation of strength near the impact surface, the delay between the arrival time and damage initiation does vary. The aggregation of the matrix damage when damage occurs easily (1 MPa) causes shock speed to dull as it progresses through a majority of the thickness, seen in Figure 6b at the 4/5th black line's arrival time compared to the other two shear strengths arrival times.

A coupled effect may be seen in matrix damage and shock stress at the 4/5th location for the 5 GPa shear strength that is not the only due to shear strength, as seen by Equation 11. There may be a mechanism occurring when shear failure is suppressed, which would explain why the orange line at 4/5th through thickness of the GRP incurs complete failure almost instantaneously while a lesser strength does not fail in the same fashion.

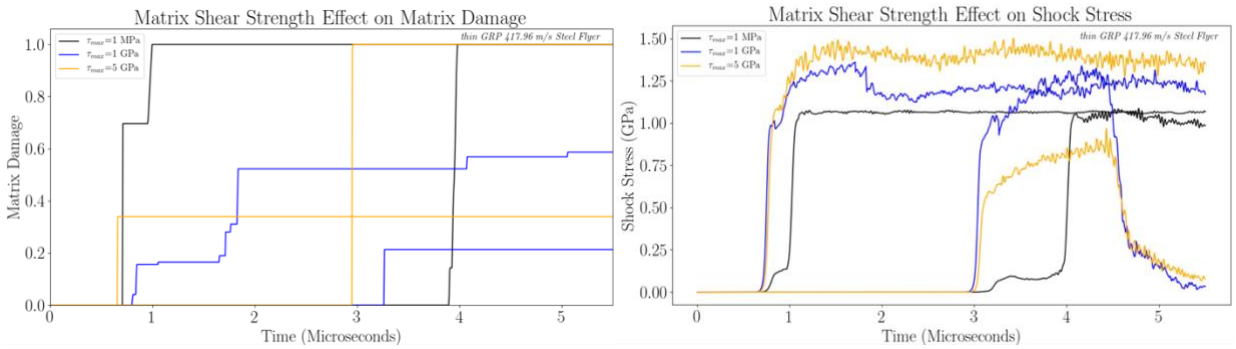

(a) (b)

Figure 6. Matrix Damage Evolution, i.e cracking, (a) and Shock Stress (b) vs time for three given Matrix Shear Strengths, 1 MPa, 1 GPa and 5GPa when all other parameters held constant. The two lines for each color signify two separate points in the GRP 1/5th and 4/5th through the thickness of the GRP.

IV.1.4 Effect of Damage Maximum (D_{max})

This parameter is the cutoff for damage, D_{max}, until the stiffness is fully degraded to a failed stiffness parameter. For low cutoffs such as 0.55, the low damage cutoff causes rapid softening, as opposed to the gradual softening seen in the 1.0 D_{max} case, see figure below. The limits of this parameter are 0-1. This paper uses 1.0 for this parameter due to the fact that the entire experiment is in compression. Meaning load should still be fully supported throughout the GRP even if matrix cracking exists.

The initial shock rise and height is affected by the damage cutoff. If the D_{max} is low, complete moduli softening should be seen when the element observes 55% damage. Figure 7b shows a softening of the loading rate for the lower D_{max} before the 100% D_{max} observes similar

softening. The aggregation of complete moduli softening affects the shock stress in the later sections of the GRP much more dramatically for the D_{max} that considers complete failure to be at 55% damage.

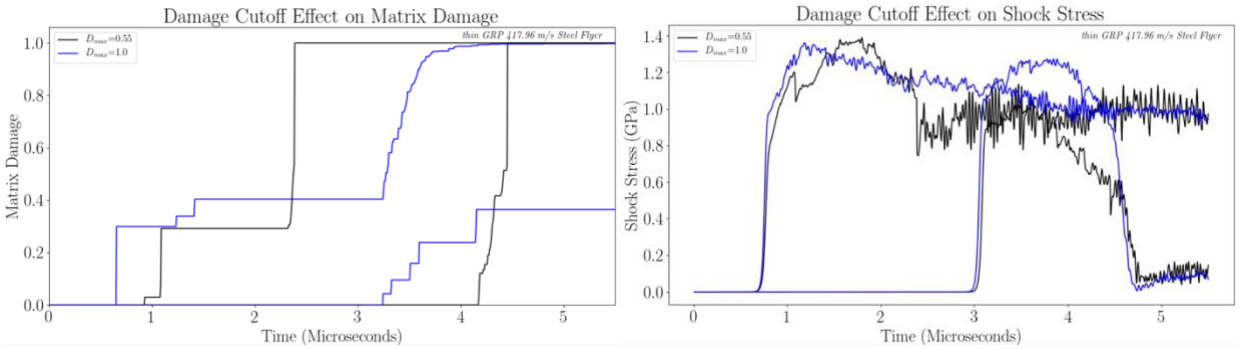

(a) (b)

Figure 7. Matrix Damage Evolution (a) and Shock Stress (b) vs time for two different D_{max} when all other parameters held constant. The two lines for each color signify two separate points, 1/5th and 4/5th through the thickness of the GRP.

IV.1.5 Initial Tangent Modulus of Unloading Once damaged

The parameter, labeled decay, is a damage parameter the controls the evolution of damage for any of the types seen in Equation 7. According to the ALE3D model description, it also helps describe the unloading tangent modulus, however as it approaches 0, numerical ringing occurs, as the tangent modulus would reach infinity. Due to this, a value of greater than or equal to 0.0909091 is recommended, but for this paper the parameter was chosen to be 5.0. Figure 8 depicts the variable ι and its effect on matrix damage evolution. As previously stated regarding Equation 7, as ι increases, the damage that occurs will significantly lessen. It also will effect the height of the shock stress. While the damage is lessened the shock stress is higher, which shows an inverse interaction between the two history variables. Figure 8 shows that

despite the damage criterion being met and exceeded due to higher stresses for ι=10, the slow climb up, controlled by ι, will yield a lower overall matrix damage. This will be true for all 4 damage variables.

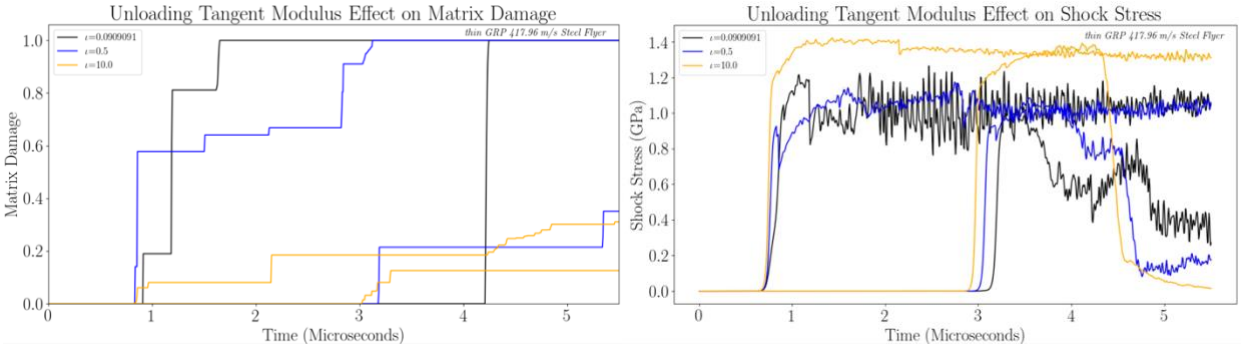

(a) (b)

Figure 8. Matrix Damage (a) and Shock Stress (b) for 3 different decay parameters while all other parameters held constant. The two lines for each color are two separate locations at 1/5th and 4/5th through the thickness of the GRP.

IV.1.6 Comparisons between Experiments and ALE3D simulations

The final parameter set was based on the capturing of the non-linearity of the velocity profile. Previous sections of this paper briefly discuss the different formulations that will be outlined in Table 4. The Epoxy-Based formulation is using the rationale that the shockwave will primarily see matrix, as the fibers will be perpendicular to the wave front, and so the matrix is the main influencer of the response, including shock velocity, and damaged moduli. Equation 6 will then use the matrix shear and bulk moduli for the K and G seen in it. The GRP-Based formulation uses the rationale that the overall stiffness of the GRP will degrade when the matrix begins to crack, so G_{ca} in Table 2 and the calculated K_{eff} of the S2 Woven Glass will be used for Equation 6. The only moduli changed for the Epoxy vs GRP based formulations were the K_{eff}

and G. This was to determine how the matrix damage and delamination damage should be degrading moduli. Fiber moduli seen in the table below are consistent, since they are not part of the matrix and delamination damage criterion seen in Equation 10-12.

All Strain rate sensitivity parameters use Equation 13 to update with respect to strain. The Volume Expansion Ratio (je) was the only variable changed between the two formulations aside from the moduli used to differentiate the two rationales.

Table 4. Parametric List of Epoxy-Based and GRP-Based Formulations

Parameter	*Versions*	
	Epoxy	**GRP**
Shear Modulus	1.33E-02	4.63E-02
Bulk Modulus	4.00E-02	1.58E-01
Beta	-2	-2
Bulk Modulus after Failure	3.09E-02	N/A
Bulk Modulus of Fiber (K_Fib)	8.69E-03	8.69E-03
K_Fib Strain Rate Sensitivity Parameter	0.1	0.1
Shear effect between fibers (ks)	3.90E-03	3.90E-03
ks Strain Rate Sensitivity Parameter	0.1	0.1
Shear Strength of Matrix (sm)	1.00E-03	1.00E-03
sm Strain Rate Sensitivity Parameter	0.1	0.1
Volume Expansion Ratio (je)	0.42	0.40
je Strain Rate Sensitivity Parameter	0.15	0.15
Tensile Strength of Fiber (T_Fib)	4.30E-02	4.30E-02
T_Fib Strain Rate Sensitivity Parameter	1	1
Compression Strength of Fiber (C_Fib)	5.00E-02	5.00E-02
C_Fib Strain Rate Sensitivity Parameter	1	1
Tensile Delamination Strength (td)	4.00E-04	4.00E-04
td Strain Rate Sensitivity Parameter	0.1	0.1
Shear Delamination Strength (sd)	1.00E-05	1.00E-05
sd SR	0.1	0.1

IV.2 Elastic Undamaged Case

The purely elastic scenario for all thin composites shown below in Figure 9 serves as a baseline case to determine if the built-in equation of state appropriately models this GRP. Given how closely the VISAR response of the experimental cases match the predicted velocities determined by the model, the model is accepted to properly predict the maximum velocity obtained by the experiments. Both the strength model and the ysmodel are used for the undamaged case, however ultimate strengths were increased to prevent damage initiation determined by the 4 damage criteria outlined in section 3.2.2 and the section below. It can be seen in Figure 9 that the impact velocity affects the steepness of the loading rate in the initial 0.1 microseconds for both experimental and computational, which gives confidence that the strain rate parameters put in place are necessary. The non-linear behavior seen in the experimental results is not captured by any of the purely elastic scenarios which may imply that the curvature in the VISAR response is due to more than just viscoelastic matrix behavior, which was speculated by Tsai et al.

IV.3 Epoxy-Based Formulation of Damage Evolution

The material model has four separate damage criteria and damage evolution variables: matrix damage, delamination damage, fiber 1 damage, and fiber 2 damage. Since fiber 1 and fiber 2 are both S2 Glass, and both are perpendicular to the shock direction, both incur damage at the same rate. However due to the experimental setup, the composite sees compression the entire time of interest to the experiment. Therefore, the fibers don’t damage significantly, if at all. Due to this fact, fiber damage is not of main interest to this paper, and will be discussed briefly in

later sections.

The delamination damage evolution is a key player to the onset of the non-linear behavior

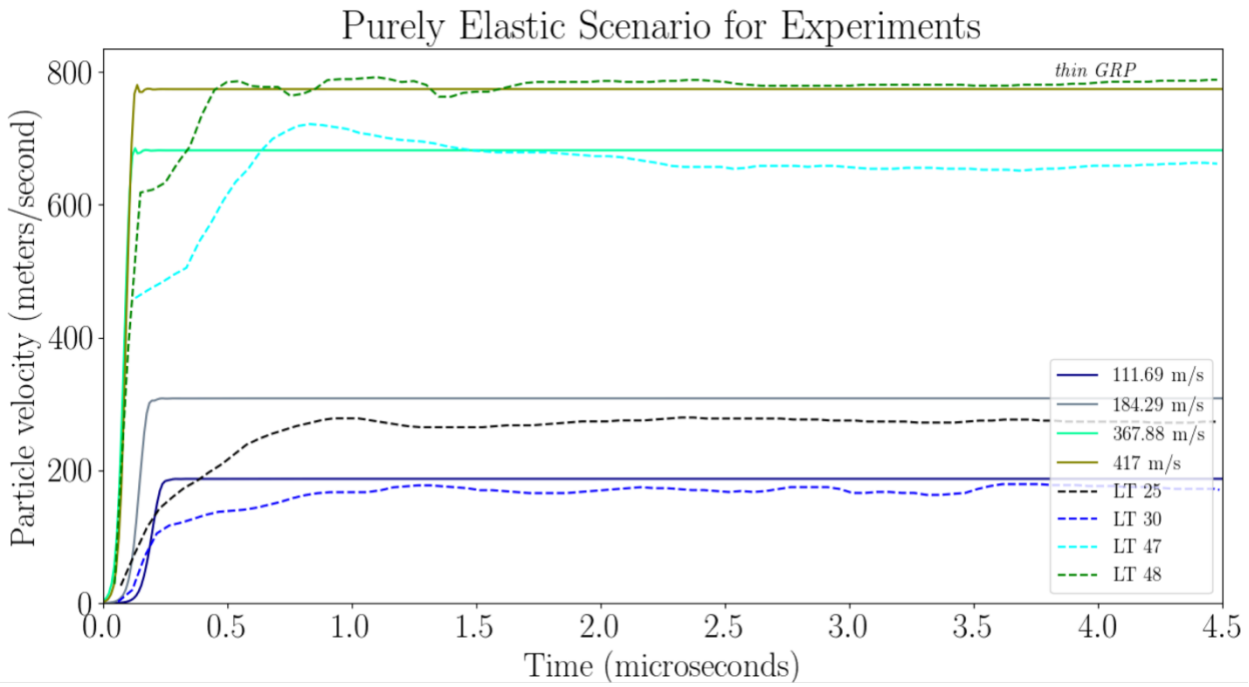

Figure 9. Free-End Particle Velocity vs Time for Purely Elastic Thin (6.8 mm) GRP. Dotted lines are experimentally determined velocity profiles. Solid lines are computational velocity profiles in an undamaged purely elastic scenario for all 4 impact velocities

depicted in Figure 10. Interestingly, if the delamination is delayed or prevented, the model predicts reaching the Hugoniot Elastic Limit (HEL) earlier. Due to this, delamination tensile and shear strengths are considered low enough to obtain the proper GRP computational response. With these delamination strength parameters supplied, the model predicts that delamination is onset and reaches total failure in less than 0.2 microseconds after shock wave arrival for every location throughout the GRP regardless of experimental impact velocity, for the thin GRP. Delamination does not hinder the shock wave given that the shock is compressive, which allows the load to still be transmitted through the GRP. While this is necessary to show the proper

velocity profile, this is not of great interest to the paper, and so will not be discussed in further detail.

Matrix damage is the last of the four damage evolution variables, and according to Equation 10 and Equation 11 it is controlled by two different criteria. Equation 11 will affect bulk

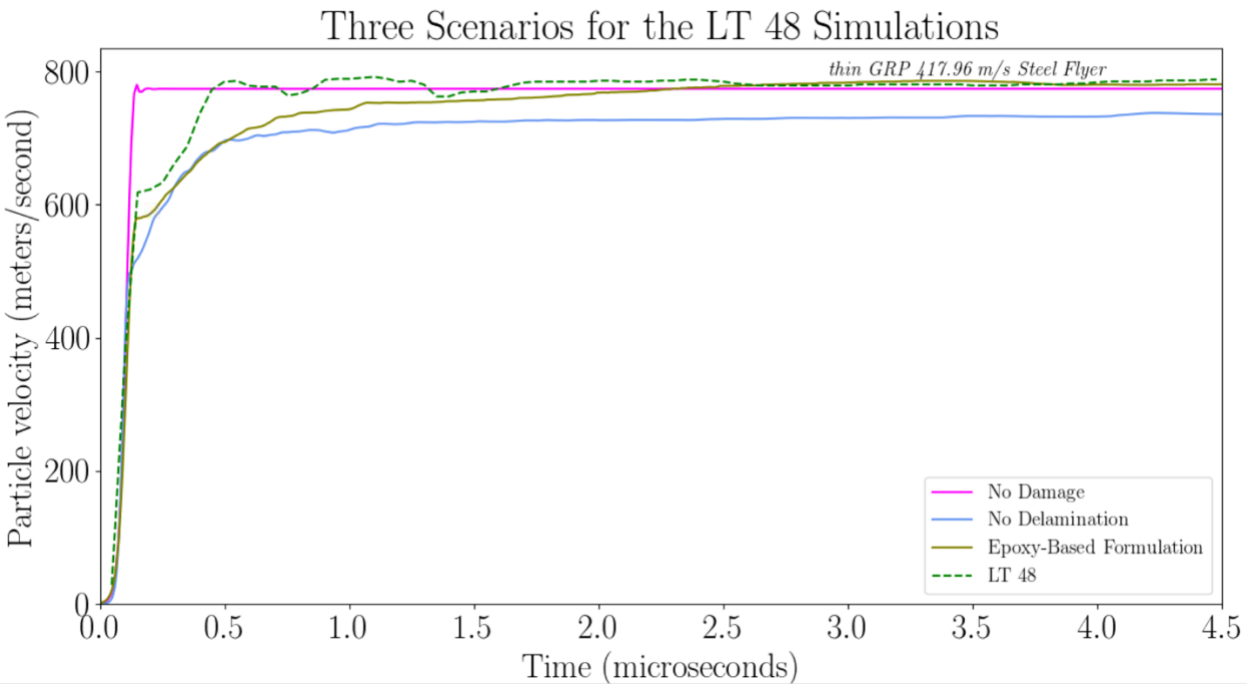

Figure 10. Comparison of Experimental VISAR response (dashed line) and 3 different computational scenarios for the LT 48 shot fired at an impact velocity of 417 m/s. The black line is the undamaged scenario, the purple is one of the accepted parametric sets, and the pink is the same parametric set with delamination damage prevented.

modulus if the R criterion is met, while the other will affect shear modulus if the criterion is met. The progression of matrix damage was unique to each impact velocity and location, unlike the total and immediate failure seen by the delamination criterion. Its evolution contributes to the non-linear shape, the height of the velocity profile, the height of the HEL, and so will be the

main damage criterion that is focused on for the interests of this paper.

Several parameter sets were found to characterize particular aspects of the GRP well. Due to the limitations of the model, and lack of machine learning, one parameter set did not capture the entirety of the GRP. Differences in how the damage evolves based on supplied parameters are outlined above in section 4.1 to help explain key differences in each model. Figure 11 below shows the best fit computational models (solid lines) compared to the experimental (dashed lines). The point at which velocity profile becomes non-linear is predicted well for all velocities aside from the 184 m/s simulation. The rise-before-plateauing effect seen in the experimental results of LT 47 and LT 48 are not captured by this model.

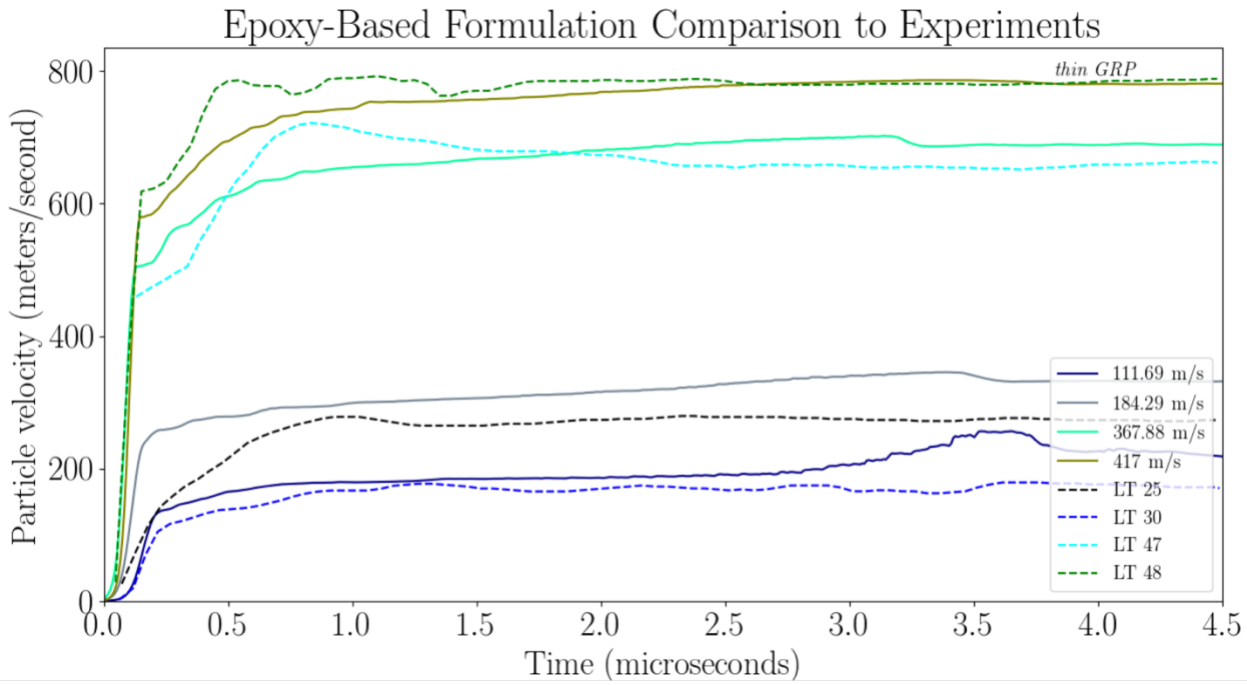

Figure 11. Epoxy-Based damage formulation parametric set found to capture experimental trends such as curvature, the non-linear initiations, and peak velocities found at the free-end of the GRP. Dashed lines are the experimental lines obtained by Tsai et al. while computational lines are solid, and labeled as the velocities of each experiment, refer to Table 1 for more information.

Figure 12, below, shows shock stress, particle velocity and matrix damage superimposed with the same time scale for the fastest experimental impact velocity. Due to oscillations in the shock stress, the damage evolution cannot be attributed to specific stresses. However, three points around 3.8 microseconds, 5.5 microseconds, and 5.8 microseconds see a jump in matrix damage, and a decrease in shock stress, this is a trend that will be seen for all cases, and will be discussed further in later sections. The particle velocity at the midpoint of the material builds up to the peak velocity after what seems like a 'reshock' scenario around 5.5 microseconds. This correlates to the same time the release wave from the free-end of the composite arrives at the midpoint of the GRP.

A general trend shows that as the stress increases, so too does the damage. However, shock stress will deteriorate as matrix cracking continues to evolve due to the degradation of the moduli that affect the deviatoric component, while pressure, however, should be relatively consistent due to force equilibrium see Figure 13. The force equilibrium seen by the two plates dictate that both the flyer and target encounter the same pressure. This compression causes the two plates to 'stick' together while the shock waves are propagating through the thickness of each plate. Once a shock wave reaches the free end, it will change sign and reflect back toward the impact surface, allowing for an unloading of the wave, seen around 6 microseconds for the midpoint of the GRP. When the release wave encounters the impact surface, the two plates no longer will be pressed together due to a compression wave.

The non-linear kink seen in the midsection of the GRP around 2 microseconds occurs before the initiation of matrix cracking at the given location in Figure 12. This shows that the matrix damage at a location may not have a role in the non-linear kink in the velocity profile seen at the same location. Therefore, it is possible the aggregation of matrix damage of previous locations adds up to form the non-linear kink shown at the free-end particle velocity to create the shape of interest.

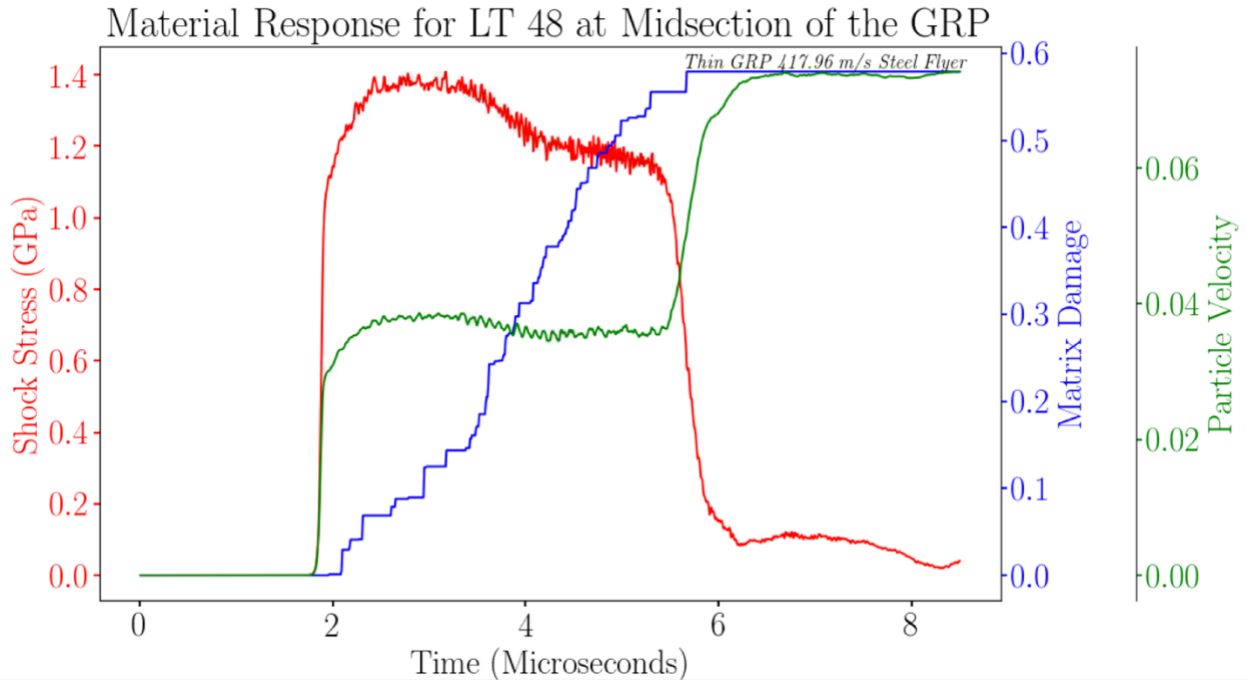

Figure 12. Shock stress (in red), Matrix damage (in blue), and Particle Velocity (in green) of the midsection of the GRP at an impact velocity of 417.96 m/s for the Epoxy-Based formulation.

The shock stress seen throughout the GRP specimen explains the damage evolution seen specifically in the matrix, such as cracking. In Figure 14, the maximum shock stress seen is at the midpoint of the composite, which should correlate with the highest damage rate seen throughout the composite. The release waves from the free end of the GRP are shown to decrease the shock stress without the intervention of the free end of the flyer nor lateral release waves, which is why the ¾ thickness decays in a short time span. As a verification, the amount of time the shockwave is seen by the ¾ thickness is half the time seen by the ½ thickness and a third of the time the shockwave is seen by the ¼ thickness due to the time required for the free end release wave to travel back through the GRP and reach those areas. If lateral release waves were present, stress attenuation would be seen in all three sections of the GRP at roughly the same interval of time,

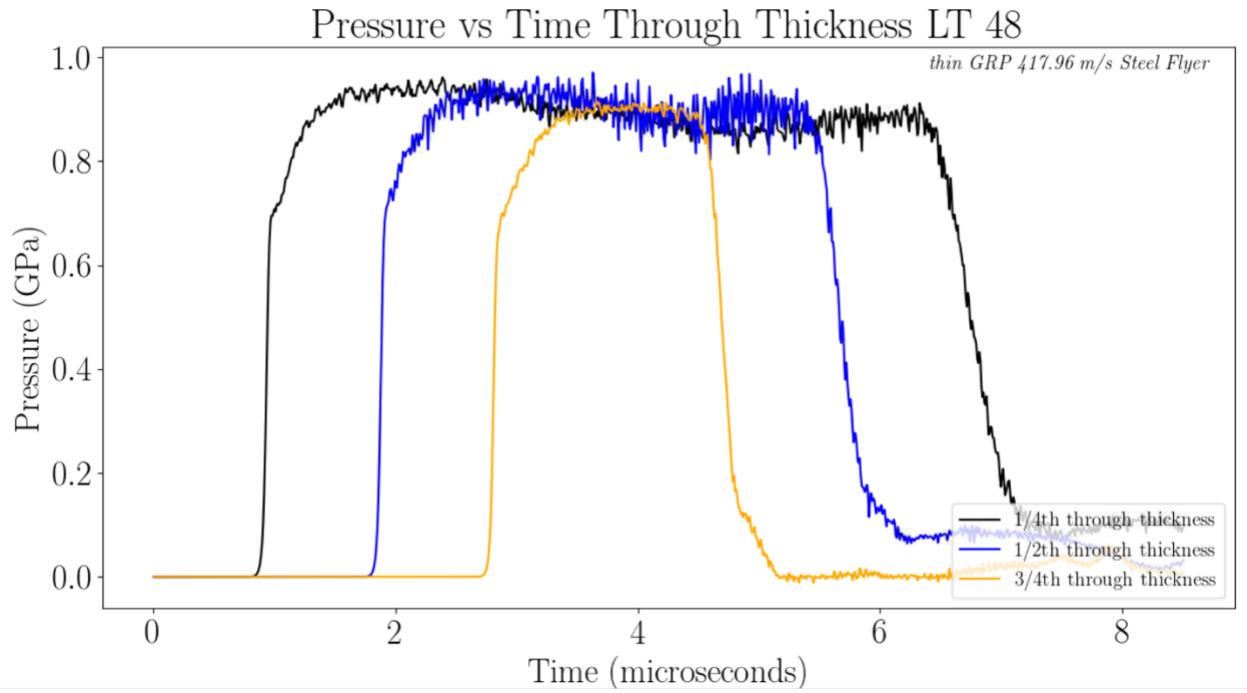

Figure 13. Pressure vs Time at varying thicknesses throughout the GRP at an impact velocity of 417.96 m/s for the LT 48 simulation.

starting with the ¼ thickness first. If the release wave of the flyer was seen in the composite, the spacing between the arrival times and departure times of the shockwave would be inconsistent. This will be discussed in later sections as an area of investigation.

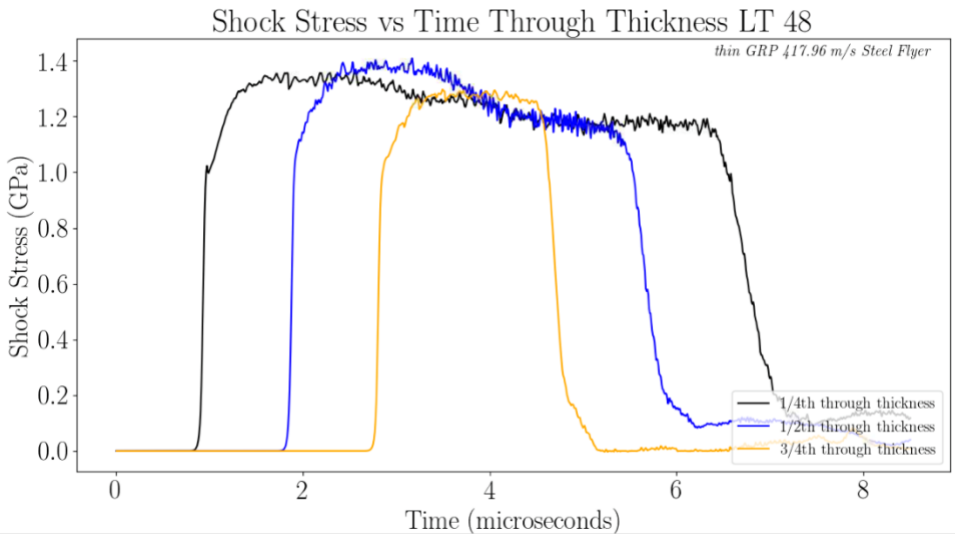

Figure 14. Shock Stress vs Time at varying thicknesses throughout the GRP at an impact velocity of 417.96 m/s for the LT 48 simulation.

The original loading line in Figure 15 below, the straight line above the jagged line, shows a linear relationship between pressure and volume (P-V), which is what the experimentalists proposed. However, when damage begins to occur, which is seen around 0.7 GPa of pressure, the curve becomes non-linear. As more damage accrues at the maximum pressure seen, roughly 0.9 GPa, the current density of the GRP continues to increase towards its maximum, note that density will always be greater than 1 due to the state of compression. As the GRP begins to relax from the load, the P-V relationship becomes jagged, most likely due to damage accrual, and it follows a more gradual slope. This is seen due to the reduction in stiffnesses due to damage, which play into the EOS P-V relations.

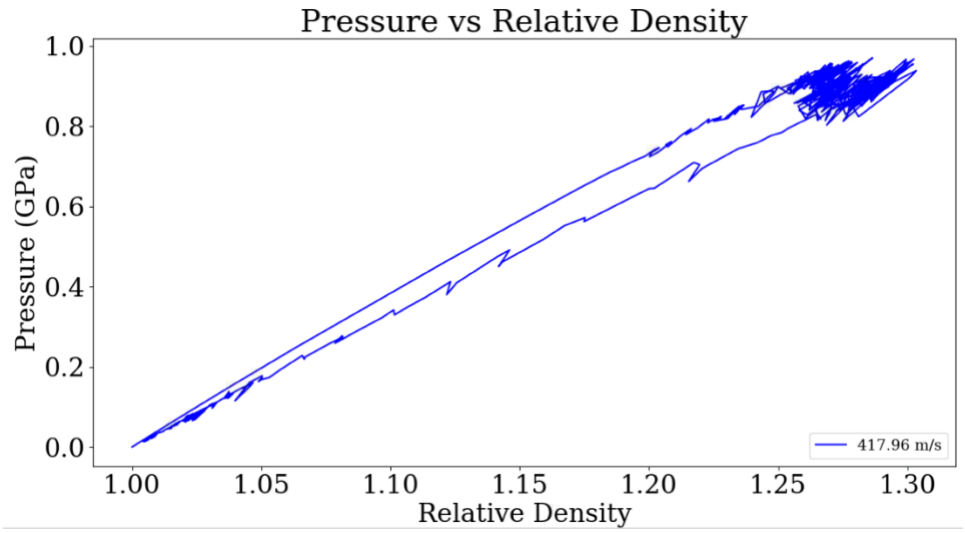

Figure 15. Pressure-Volume relations shown through relative density at the midpoint of the GRP for the impact velocity of 417.96 m/s for the LT 48 simulation.

The delamination damage seen below in Figure 16 shows the composite immediately failing under this criterion. The initiation of damage seen around 1 microsecond at the ¼ thickness is the same time that pressure arrives, see Figure 13, in the ¼ thickness section of the GRP. Each quarter thickness after shows the same behavior. Since the composite is in compression, the composite still transmits the load through the thickness after delamination. It is seen in Figure 10, that increasing the delamination strength will lower the peak velocity in the velocity profile. Given the agreement of computational and experimental shown in Figure 11, it is likely large amounts of delamination occurred in the experiments in the first 3 microseconds, which would not be able to be differentiated from the delamination occurring by tensile release waves the GRP encounters before posthumous recovery of the specimen in the experimental setting.

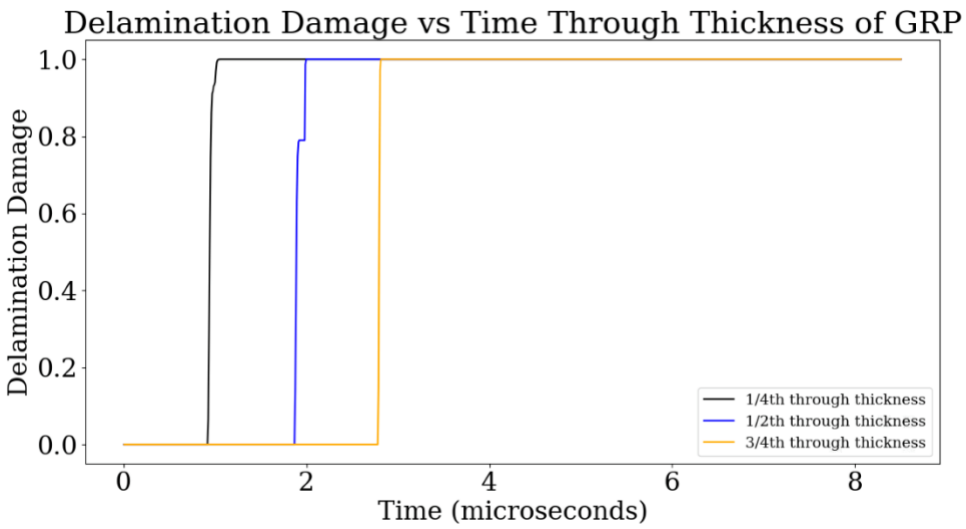

Figure 16. Delamination Damage vs Time at varying thicknesses throughout the GRP at an impact velocity of 417.96 m/s.

Intuitively, matrix cracking would seem to be most prevalent near the impact surface. However, Figure 17 depicts that the midpoint of the GRP has a higher damage accumulation than close to the impact surface. This can likely be explained by the shock stress seen in Figure 14, where the ½ thickness sees about 50 to 75 MPa more than the ¼ thickness. Both of these see around 50-125 MPa more than the ¾ thickness which could explain the lack of similar damage evolution in the ¾ thickness section. The amount of local matrix damage in the GRP should decrease at a location further away from the impact plane, due to the shock front dulling as damage aggregates. This is also why the shock stress seen by the 3/4th thickness is noticeably less than that of the other two locations.

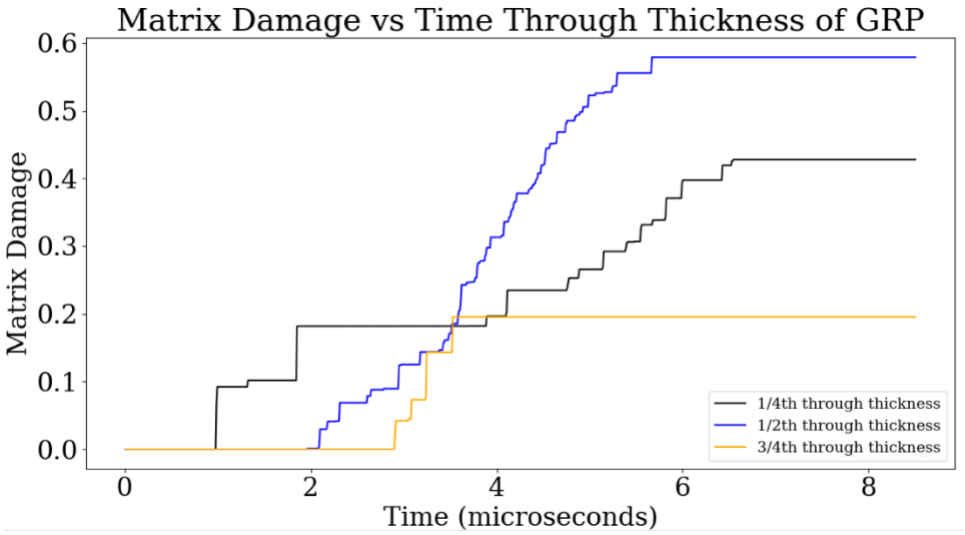

Figure 17. Matrix Damage vs Time at varying thicknesses throughout the GRP at an impact velocity of 417.96 m/s.

No fiber damage is seen due to the compressive stress state the composite is subjected to. Release waves from the flyer and free end of the GRP will not change this response and will be discussed in detail in later sections of this paper.

IV.4 Full GRP Moduli Damage Formulation

Due to the Hugoniot stresses not matching calculated stresses by Tsai et al, an investigation into the damage formulation was launched. We postulated that if the matrix cracked, it could deteriorate more than just the matrix stiffness that the shock wave propagates through. Instead, it affected the full GRP bulk and shear moduli, which is inclusive of the fibers. This is contrary to the thought that since fibers are perpendicular to the wave front, the wave front doesn't "see" the fibers as a whole.

In order to simulate this, matrix cracking would actually decrease the overall GRP effective bulk modulus and shear modulus seen in Equation 6. The result was a proper Hugoniot stress as predicted by Tsai et al, as well as a more appropriate shock velocity, correlating to the paper as well. See Table 5 below for comparisons, Tsai et al. found the shock stress to be 2.308 GPa for the LT 48 experiment impacting the specimen at a velocity of 417.96 m/s. The 'Epoxy No Damage' and 'Fiber No Damage' cases (seen as first and last case in the table), were used as a verification of accuracy and also an upper and lower bound for wave speeds and shock stresses that should be seen for the 417 m/s experiment. These two simulations used either epoxy or fiber properties for both their strength model and their yield surface model respectively. The two separate Epoxy Formulation and GRP Formulation parameter sets are outlined it Table 4. Comparing Tsai et al's findings of 2.308 GPa shock stress and a shock velocity of 0.3453 cm/microsec for the LT 48 case, only the GRP Formulation with damage is accurate with an error of 3.98% for shock stress and 0.058% error for shock velocity.

Table 5. Various Damage Formulations for the LT 48 Experiment Simulation

Case	Free Surface vel from Graph (cm/microsec)	Shock Stress Calculated (GPa)	Peak Shock Stress on Graph @ GRP Midpoint (GPa)	Shock Velocity Based on Arrival times in Simulations (cm/microsec)
Epoxy No Damage	0.0785	1.087148009	1.18	0.2066
Epoxy Formulation GRP No Damage	0.078	1.43175474	1.41	0.1874
Epoxy Formulation GRP Damage	0.0784	1.393021392	1.37	0.1814
GRP Formulation Damage	0.0734	2.483982615	2.4	0.3455
All Fiber No Damage	0.0602	4.73859282	4.82	0.6608

The GRP-based damage formulation parameter set was relatively similar to that of the epoxy-based damage formulation parameter set of section 4.3 aside from slight modifications to the je variable, and of course the shear and bulk moduli that were to be damaged once matrix damage began to occur. No strain rate variables were altered, and all strain rate variables increase logarithmically to the originally defined variable. The particular je for each scenario was chosen so that the majority of the velocity profiles' maximum matched the height of the VISAR data. Interestingly enough, the curvature seemed to be less manipulatable, and so the distinct kinks seen in Figure 11. Epoxy-Based damage formulation parametric set found to capture experimental trends such as curvature, the non-linear initiations, and peak velocities found at the free-end of the GRP. Dashed lines are the experimental lines obtained by Tsai et al. while computational lines are solid, and labeled as the velocities of each experiment, refer to Table 1 for more information. are non-attainable with this parameter set. Instead, the goal became to

match the initiation of non-linearity in the velocity profile, it is best seen with LT 30 and LT 47 and their respective simulations. LT 31 is included in the list of these simulations because the simulation's maximum free particle velocity agreed with the experimental results. This is also the case for simulations LT 44 and LT 51 seen in the thick GRP velocity profiles in Figure 19 below.

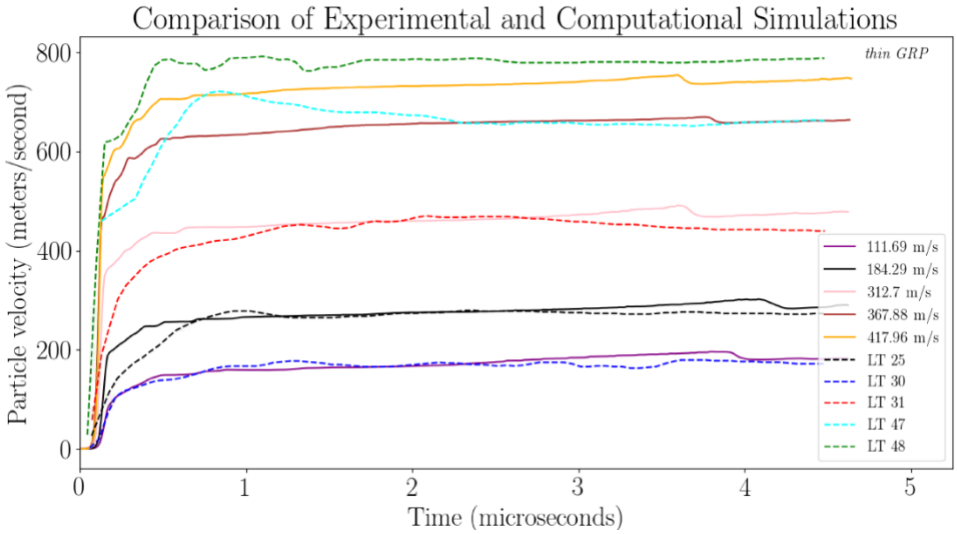

Figure 18. GRP based damage formulation parametric set found to capture experimental trends such as curvature, the non-linear initiations, and peak velocities found at the free-end of the thin 6.8 mm GRP cases. Dashed lines are the experimental lines obtained by Tsai et al. while computational lines are solid, and labeled as the velocities of each experiment, refer to table 1 for more information.

There are gradual rises seen in most of the velocity profiles for any of the formulations and regardless of thickness. These can only be suppressed by turning off matrix damage. Initial thoughts had to do with delamination causing re-shocking, but these 'bumps' were still observed when delamination is removed. Instead the belief is re-shocking occurs due to matrix cracking causing the relative density to decrease, which will in turn cause small amounts of re-shocking from impedance mismatching due to density differences throughout the material. The tiny shock

wave seems to be generated close to the middle of the GRP and propagates out when looking at the post-processing videos, however nothing significant or obvious is seen in the shock stress time history in below. When comparing similar impact velocities of the two different thicknesses, the initial slope and beginning of curvature seems to be less 'stiff' for the thicker composite over the thinner composite, this may have to do with damage evolution occurring throughout the thickness of the GRP as the shock front progresses. This phenomenon will be discussed in more detail below.

The matrix damage doesn't seem to necessarily correlate with huge jumps shock stress or relative density. Figure 20 was created to visualize the states of shock stress and volume reduction at which damage increases. The location at 1/4$_{th}$ through thickness of the small GRP was of interest due to 1) the 'stair stepping' nature of the matrix damage, 2) the shock stress staying consistent from this point on throughout the rest of the thickness of the GRP, and 3) the fact that it was far enough away from the impact surface to not carry numerical artifacts from it. Shear may have contributed nominally to the damage, but when changing the strength at which shear-based matrix damage occurred, little to no response changed via the matrix damage graph. Due to that, only variables that were in Equation 11 played a role in matrix damage. The initial matrix damage occurs shortly after the arrival of the shock wave, and approximately at the time the shock stress becomes non-linear, which does not necessarily coincide with the relative density non-linear initiation. The two major events of matrix damage, which have dotted

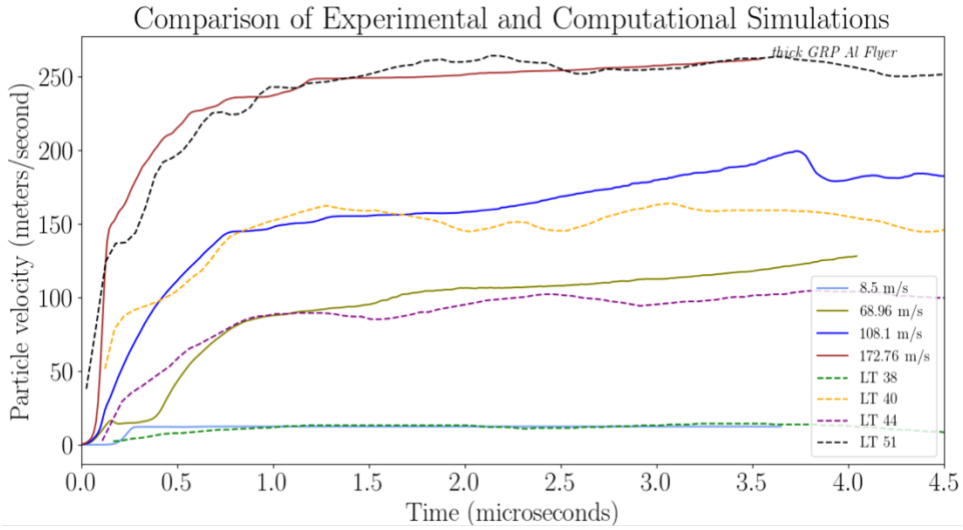

Figure 19. GRP based damage formulation parametric set found to capture experimental trends such as curvature, the non-linear initiations, and peak velocities found at the free-end of the thick 13.6 mm GRP cases.

lines leading from them to the same state of shock stress and relative density at a given time, right after the initial damage seem to occur right after a slight drop in stress. Due to the oscillatory nature of the shock stress however, this can't be said to cause the damage, since small stair stepping matrix damages is not seen throughout the entire time despite the constantly fluctuating stress. The relative density also saw small sharp drops during and after the matrix damage occurred. Since the shock stress oscillates, unfortunately so too will the relative density, but the two later cases of matrix damage shed extra light onto the damage mechanism. After the unloading of the shock stress, two jumps in matrix damage are seen. Both of which have a small drop in relative density during and after the damage occurs. This may be explained by the comment in the previous paragraph about coalescing cracks once the matrix is no longer compressed.

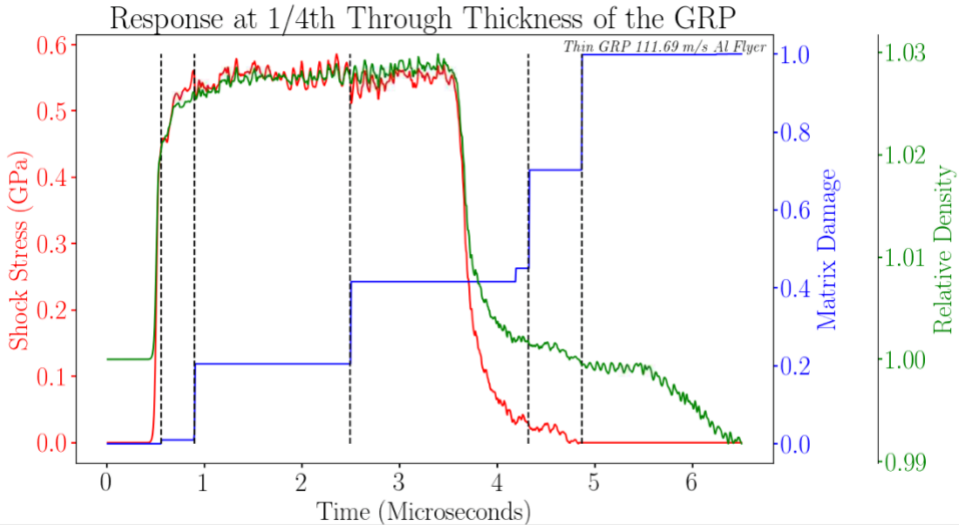

Figure 20. Tri-y axial graph correlating shock stress (red), matrix damage (blue), and relative density (green) at specific points where matrix damage for the thin GRP LT 30 Simulation.

The velocities that the shock stresses of Figure 21a and b are comparable, so that observations may be made about the thickness's role in the GRP material response. The precursor delay is more evident in the thick composite, Figure 21b, than in the thin composite, Figure 21a. Note the almost linear behavior at the 1/16th thickness shock stress for both, and as the deterioration of the shock front due to damage accumulation, the linear region becomes smaller. The 7/8th thickness of the 13.6 mm GRP is almost completely a smooth curve, which is seen as much more of an exaggeration than the thin composite. In fact, the midpoint of the thick GRP, or the red line, in Figure 21 below, roughly begins the same smoothing shape as the olive line, in Figure 21above, around the same height which is the 7/8th thickness of the thin GRP. The discrepancies of the two is most likely due to the extra 1/8th thickness the red line has, given that its length is 6.8 mm while the thin composites 7/8th is 5.95 mm. This explains why the red line in Figure 21 initiates the non-linearity just a little bit before the olive line of the thin composite.

A phenomenon called precursor decay is predicted in the thin GRP at 111.69 m/s as seen

in Figure 21, which is most likely due to the damage accumulating as the shock wave moves through the GRP cracking up the matrix and causing delamination. The viscoelastic nature may also have some play in this response in the lower velocity experiments, as our preliminary results suggested when the specimen was subjected to a load fast and was allowed later to relax. The phenomenon will be discussed shortly below in further detail.

Pressure-Volume relations seen below in both thick and thin GRP simulations do not resemble Figure 15 in section 4.3. It seems that the damage evolution seen below play a much smaller role in preventing the pressure-volume to be approximately linear. The LT 40 simulation shows two separate lines, more easily distinguished than its thinner counterpart LT 30, due to two active damage criteria. The line that goes back to the origin shows a much less linear path due to damage accumulation, while the undamaged portion on the pressure-volume relationship seems to be a straight line.

The precursor delay is seen much more dramatically in the initial strain rate in Figure 21. As the shock wave travels through the composite, the strain rate gets lower and lower, and is seen more apparently in the LT 40 case due to the extra thickness. The reason the thin composite shows a much higher initial straight rate is due to the fact that its $1/8_{th}$ thickness is half of the distance to the impact surface.

A trend is not easily seen by the damage of the matrix in Figure 21. However, most of the thicknesses chosen show to have an initiation of damage approximately 0.01-0.2 microseconds after the wave arrives at the location when looking at arrival times of shock. This shows that damage isn't happening instantaneously at the shock wave front. Instead it generally correlates with the point at which the shock stress becomes non-linear, although this isn't all of the

scenarios, see the 3/4th thickness damage and shock profiles. The major climb in damage is seen in most of the selected points throughout the thickness when the release wave has reached the section, allowing it to decompress. Perhaps this is seen as allowing the cracks to open, since they are no longer in compression, which would allow for the relative density to normalize. If the cracks are allowed to open due to the roughly 0 stress state, they may coalesce if a large number of microcracks are nearby, which would explain the increase to fully damaged matrix despite the shock wave unloading. There were small portions of the sections the GRP close to the impact surface that saw tension shortly after the unloading shock wave, such as the 1/8th through thickness line for LT 40. This may have been due to the release wave reflecting back due to impedance mismatch of the aluminum flyer and the GRP.

Figure 22 depicts the Hugoniot curve, a description of the pressure-volume relation, found at the midpoint of the GRP. It correlates the maximum shock stress and the respective volumetric strain, defined as $1-V/V_o$, of each experiment's simulation. All thin GRP experimental velocities discussed in this paper were used to construct this as well as 500 m/s and 700 m/s to ensure the polynomic nature of the Hugoniot curve was captured. Tsai et al proposed a linear pressure-volume relation in their paper when correlating the shock velocity and particle velocity. This could be used as a rough approximation for the maximum stress seen by, however, each of the data points are slightly off the line based on elastic wave speed. As you increase in velocity, the approximation becomes less accurate.

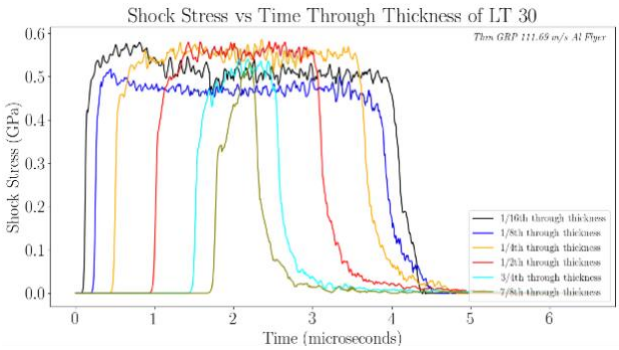
Shock Stress vs Time Through Thickness of LT 30
Thin GRP 111.69 m/s Al Flyer
Shock Stress (GPa)
Time (microseconds)
1/16th through thickness
1/8th through thickness
1/4th through thickness
1/2th through thickness
3/4th through thickness
7/8th through thickness

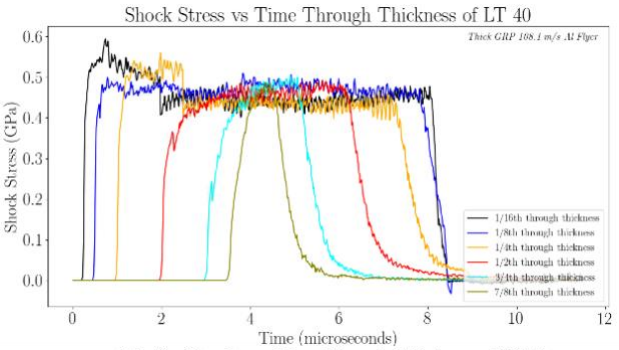
Shock Stress vs Time Through Thickness of LT 40
Thick GRP 108.1 m/s Al Flyer
Shock Stress (GPa)
Time (microseconds)
1/16th through thickness
1/8th through thickness
1/4th through thickness
1/2th through thickness
3/4th through thickness
7/8th through thickness

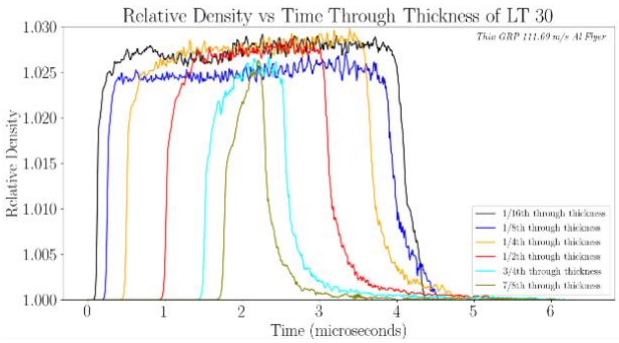
Relative Density vs Time Through Thickness of LT 30
Thin GRP 111.69 m/s Al Flyer
Relative Density
Time (microseconds)
1/16th through thickness
1/8th through thickness
1/4th through thickness
1/2th through thickness
3/4th through thickness
7/8th through thickness

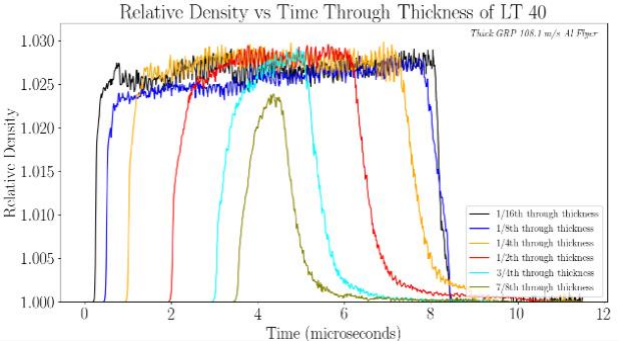
Relative Density vs Time Through Thickness of LT 40
Thick GRP 108.1 m/s Al Flyer
Relative Density
Time (microseconds)
1/16th through thickness
1/8th through thickness
1/4th through thickness
1/2th through thickness
3/4th through thickness
7/8th through thickness

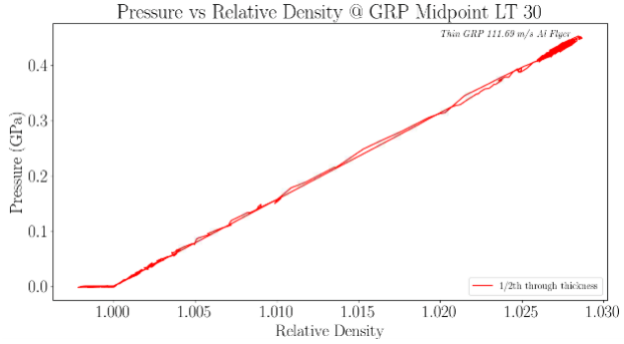
Pressure vs Relative Density @ GRP Midpoint LT 30
Thin GRP 111.69 m/s Al Flyer
Pressure (GPa)
Relative Density
1/2th through thickness

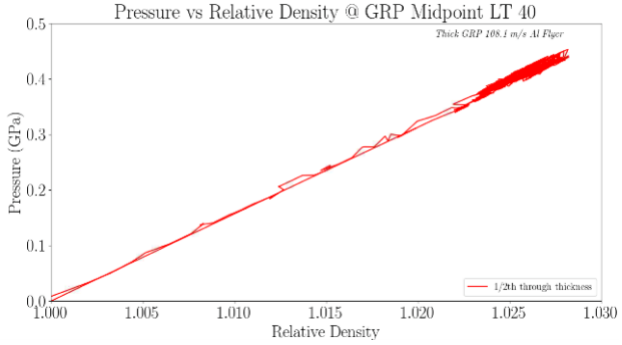
Pressure vs Relative Density @ GRP Midpoint LT 40
Thick GRP 108.1 m/s Al Flyer
Pressure (GPa)
Relative Density
1/2th through thickness

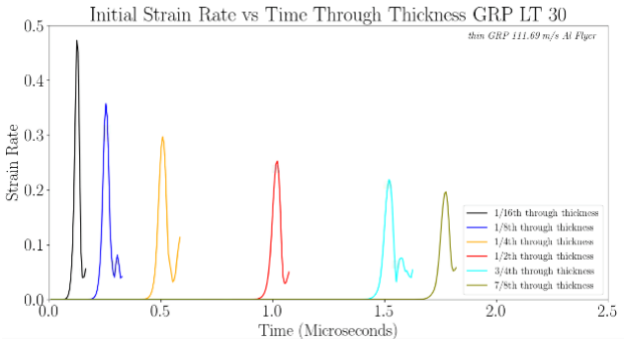
Initial Strain Rate vs Time Through Thickness GRP LT 30
thin GRP 111.69 m/s Al Flyer
Strain Rate
Time (Microseconds)
1/16th through thickness
1/8th through thickness
1/4th through thickness
1/2th through thickness
3/4th through thickness
7/8th through thickness

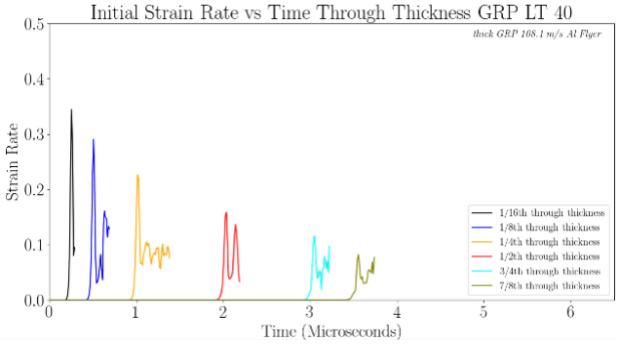
Initial Strain Rate vs Time Through Thickness GRP LT 40
thick GRP 108.1 m/s Al Flyer
Strain Rate
Time (Microseconds)
1/16th through thickness
1/8th through thickness
1/4th through thickness
1/2th through thickness
3/4th through thickness
7/8th through thickness

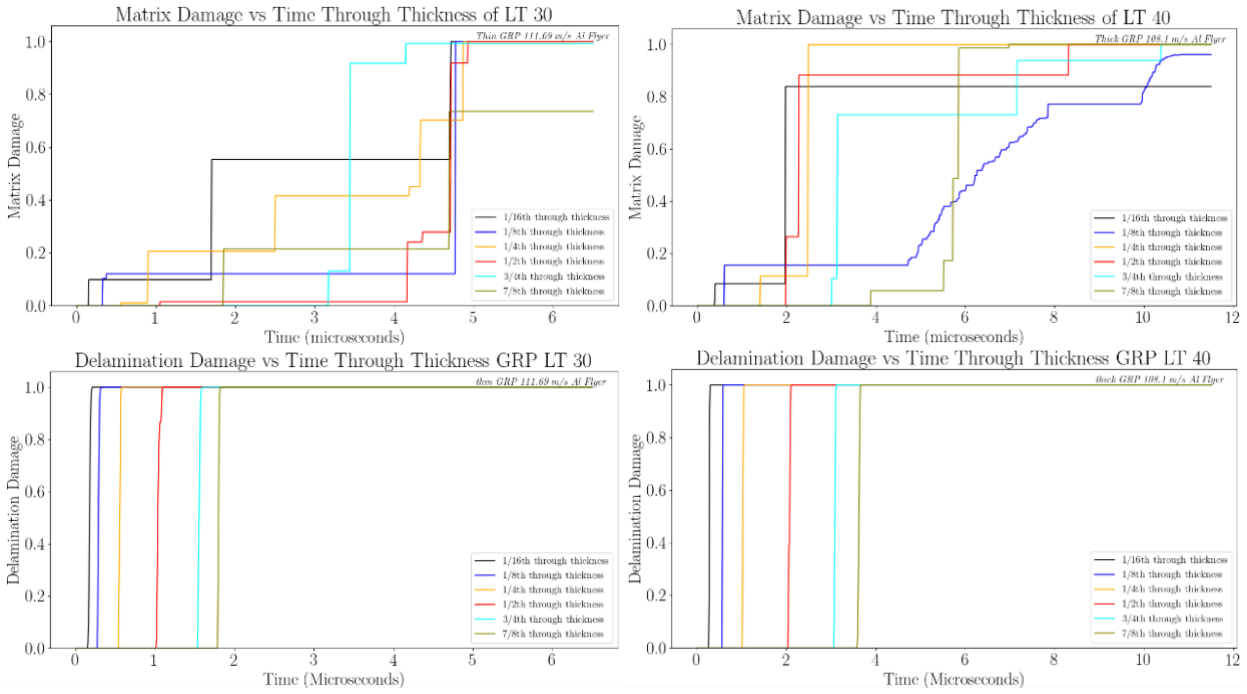

Figure 21. Comparisons of shock stress, relative density, and matrix damage through the thickness of the GRP between LT 30 and LT 40 due to similar velocities but different GRP thicknesses.

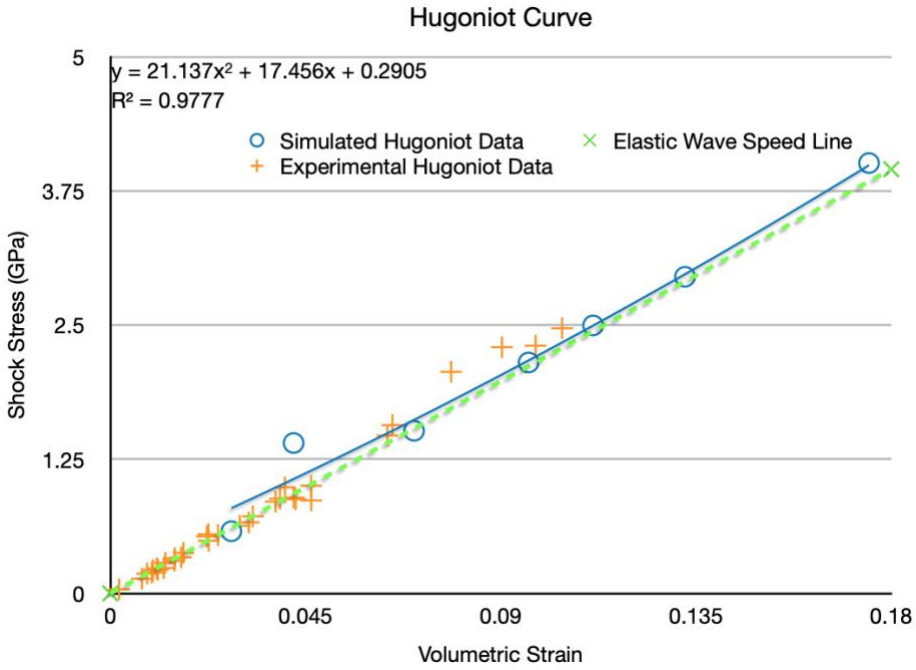

Figure 22. Hugoniot Curve constructed using the thin GRP simulations. Simulation Data includes velocities of 111.69, 184.29, 312.7, 417.96, 500, 700 m/s. Elastic Wave Speed Line was constructed using bulk and shear moduli of the GRP. Experimental Data obtained from Tsai et al [1].

Tsai et al. [1] predicted that the non-linear behavior seen in the velocity profiles captured by their VISAR was due to viscoelastic properties. Figure 23 shows the difference in a purely viscoelastic material with no damage, and a hyperelastic progressive damage model. A purely elastic version was used, because Tsai et al. predicted viscoelastic, not viscoplastic behaviors. The result seen below, is a gradual rise in the free surface velocity, as well as a gentle smooth non-linear portion when the maximum velocity is reached. Neither of these are traits of the experimental data seen below. The Viscoelastic model doesn't have an obvious HEL that can be compared with the damage model or the experimental data.

We can say with confidence, that the non-linear response is not just do to viscoelastic

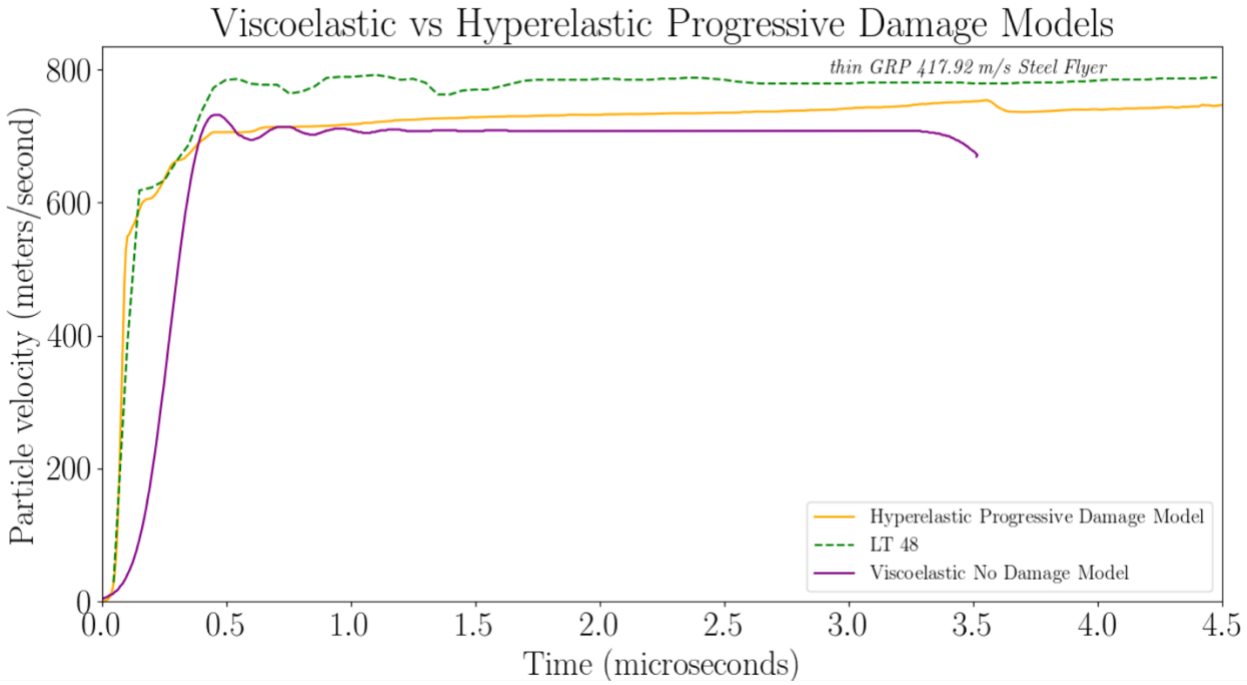

Figure 23. Two different material models predicting the velocity profiles of the LT 48 experiment. The hyperelastic damage model uses the parameterization shown above, while the viscoelastic model uses G, K, and a Relaxing ratio.

behavior that Tsai et al [1] predicted. Instead it heavily correlates with matrix damage and delamination damage as previously predicted in this section.

CHAPTER V

SUMMARY AND CONCLUSIONS

The shock propagation in a S2-glass woven composite laminate was modeled using the ALE3D finite element code. A continuum damage mechanics based hyperelasticity constitutive equation described the shock response of the laminate (or GRP) under compressive loading. Since the architecture of the woven composite is complex, a simplistic approach in which a $0_0/90_0$ unidirectional layup was modeled while the volume fractions of S2 glass fiber and the polyester (or epoxy) matrix were kept the same. Though the damage model formulation includes a variety of damage modes as described in section 3, the present work considered only the 2 failure modes: matrix cracking/damage, and intra-ply delamination. These two modes are captured by modeling the degradation of shear and bulk moduli.

Damage initiation is assumed to occur when the applied strain exceeds a critical strain value that can be determined from experiments. However, the critical value depends on the failure modes associated with fibers and matrix under both tension and compression. The damage evolution or growth law is based on an exponential equation that enables the damage to increase from 0 to 1. To understand damage evolution and shock wave propagation in GRP, the shock response of an epoxy (or matrix only) target was modeled in ALE3D and comparisons were made between the two responses.

The velocity profiles do not correlate fully in the initiation region of the non-linear velocities for the GRP-based formulation, instead the epoxy-based formulation showed more

accurate results for the higher velocity behaviors. However, based on the shock velocity and shock stress histories in the GRP for both formulations, the degradation of the matrix due to cracks does not significantly influence the stress amplitudes. However when the release wave from the target's stress free back surface propagates back into the target, the incipient damage level reaches the maximum (d = 1). The GRP's moduli will deteriorate at a faster rate than the epoxy-based formulation due to matrix cracking, which causes an underestimation of stiffness degradation if only the matrix moduli are used. Fiber damage is not prevalent in the timespan relevant to the plate impact tests due to the target plate being in compression, but delamination prevents any region where tension would occur in a traditional material, which in turn does not allow for fiber damage. Delamination occurs almost instantaneously as the wave arrives at a location due to shear loading (difference between the shock stress and the lateral stress). Since the GRP is under multiaxial compression state, the delamination damage does not separate the plies. Therefore, spall type failure is not expected to occur in GRP. Also, the delamination response of the GRP under compression does not influence the matrix cracking. From the simulations, any interplay between these two modes is not observed. The small rises (increases) in particle velocity seen in the velocity plots are due to the matrix-damage-caused incremental stress releases.

Precursor delay phenomenon was noticed in the ALE3D simulations as the shock propagates into the target plate prior to any damage initiation and growth. The strain rate decay as the shock wave propagates away from the impact plane causes the precursor decay

phenomena.

Tsai et al. [1] speculated that the nonlinear portion of the VISAR data could be due to viscoelastic response of the GRP. The preliminary investigation from the plate impact simulation from the ALE3D code using a viscoelastic constitute response suggests that the elastic nonlinear strains alone is not sufficient enough to match the so called "nonlinear portion" of the VISAR data. From the current study, it appears that modeling of strain rate dependent (viscous) damage in the GRP under shock compression is necessary to capture several salient features of the VISAR signal.

Based on their experimental data interpretation by Tsai et al., [1], they did not observe the elastic – plastic transition within the range of impact velocities. However, when high velocity data of Dandekar et al., was included in the Hugoniot plot, the HEL was very visible with a value of about 1.5 to 2 GPa. In ALE3D simulations especially for the steel flyer plate, the free surface velocity history showed transition from elastic to inelastic due to damage initiation in GRP under compressive loading. In metals and ceramics, this transition point is always considered to be the HEL. This does not seems to be true for GRP type composites. By constructing the Hugoniot curve as locus of shock stresses at different velocities, it is clear that the beginning of the nonlinear portion in the particle velocity plots for GRP does not mean that it is the HEL point. In general, The CDM based hyperelastic constitutive model developed at LLNL reproduced the VISAR data of Tsai et al., [1] reasonably well. The ALE3D simulations using one set of model parameters predicted the VISAR signals for both thin (~7 mm) and thick (~13 mm) GRP at

different velocities.

Based on the current ALE3D analyses of shock wave propagation in a complex layered polymeric composite solid, there are several unanswered questions related to the definition of Hugoniot Elastic Limit, precursor decay, and inelastic strains in GRP. More modeling efforts are required to fully explain the damage initiation and propagation behind the shock wave and how they influence the incremental unloading and reshocking of the shock stress and particle velocity s seen in the time history plots. The main advantage of the empirical damage model used in this study is the need for determining very few model constants in terms of critical strains required to initiate and grow damage under different fiber / matrix failure modes. Though the relatively low velocity VISAR data of Tsai et al [1] were very well predicted by the hyperelastic damage model, further validation is needed through the use of high velocity date of Dandekar et al [15].

BIBLIOGRAPHY

BIBLIOGRAPHY

1. Liren Tsai, Fuping Yuan, Vikas Prakash, and Dattatraya P. Dandekar, “Shock compression behavior of a S2-glass fiber reinforced polymer composite, “ Journal of Applied Physics, Vol: 105, 093526 (2009); https://doi.org/10.1063/1.3124622
2. Kim, J. K.; Sham, M. L. (2000): Impact and delamination failure of woven-fabric composites. Composites Science and Technology, vol. 60, pp. 745-761.
3. N. Razali, M.T.H. Sultan, F. Mustapha, N. Yidris, and M.R. Ishak, “Impact Damage on Composite Structures – A Review,” The International Journal Of Engineering And Science (IJES), Vol 3, Issue 7, pp. 08-20, 2014.
4. Hashin, Z.: Failure criteria for unidirectional Fiber composites. J. Appl. Mech. 47, 329–334 (2015)
5. G.A.O.Davies, D.Hitchings, and G.Zhou, “Impact damage and residual strengths of woven fabric glass/polyester laminates,” Composites Part A: Applied Science and Manufacturing, Volume 27, Issue 12, pp. 1147-1156, 1996.
6. Asay, J.R. and Lipkin, J. Journal of Applied Physics 1978; 49: 4242.
7. McQueen, R.G., Marsh, S.P., Taylor, J.W., Fritz, J.N., and Carter, W.C., 1970, "The equation of state of solids from shock wave studies," High Velocity Impact Phenomena (R. Kinslow, Ed.). New York: Academic Press, pp. 293- 417; 515-568.
8. Orson l. Anderson, “Equations of state of solids for geophysics and ceramic science,” Book, Chapter 12 on Shocked Solids, pp 307 – 326, Oxford University Press 1995
9. T. Nicholas, and A.M. Rajendran, "High Strain Rate Behavior of Materials," a Chapter in 'High Velocity Impact Dynamics,' edited by J. Zukas, John-Wiley & Sons, Inc., pp. 127-296, 1990.
10. N. Chandra, X. Chen, and A.M. Rajendran, “The Effect of Material Heterogeneity on the Shock Response of Layered Systems in Plate Impact Tests,” Journal of Composites Technology & Research, pp. 232-238, 2002.
11. Tsou F. K. and P. C. Chou, 1969. “Analytical Study of Hugoniot in Unidirectional Fiber Reinforced Composites” , Journal of Composite Materials, 3, 500-514.12.
12. Munson D. E. and Schuler K. W., 1971. “Steady Wave Analysis of Wave Propagation in Laminates and Mechanical Mixtures”, Journal of Composite Materials, 5, 286-304.
13. J.M. Boteler, A.M. Rajendran, and D.J. Grove, “Shock Wave Profiles in Polymer Matrix Composites,” in Proceedings of the American Physical Society Conference on “Shock Compression of Condensed Matter”– 1999,” Eds: Furnish, Chhabildas, and Hixson, pp. 563-566, APS Press, 2000.

14. L.Tsai, V. Prakash, A.M. Rajendran, and D.P. Dandekar, “Structure of Shock Waves in Glass Fiber Reinforced Polymer Matrix Composites,” Applied Physics Letters, Vol. 90, Jan 2007.
15. Dandekar DP, Hall CA, Chhabildas LC et al (2003a) Shock response of a glass-fiber-reinforced polymer composite. Compos Struct 61(1–2):51–59.
16. P. Kumar and R. J. Clifton, “A star-shaped flyer for plate-impact recovery experiments,” Journal of Applied Physics 48, 4850 (1977)
17. Rajendran, A. M., Brar, N. S., & Khobaib, M., "Effects of Dynamic Pre-Strain on the Subsequent Tensile Flow Strength," in Proceedings of the American Physical Society Conference on “Shock Compression of Condensed Matter” – 1989”, S.C. Schmidt, J.N. Johnson, and L.W. Davison (Editors), Elsevier Science Publishers, pp. 401-404, 1989.
18. G.T. Gray III, “Shock recovery experiments: An assessment,” Proceedings of the American Physical Society topical conference on shock compression of condensed matter, Albuquerque, NM, USA, 14-17 Aug 1989.
19. D.P. Dandekar, J.M. Boteler, and P.A. Beaulieu, Composite Science Technology, %*, pp. 1397 (1997).
20. M.I. Barham, M.J. King, G. Mseis, and D.R. Faux, “Hyperelastic Fiber-Reinforced Composite Model With Damage, a technical report, Lawrence Livermore National Laboratory, LLNL-MI-644243, September 30, 2013.
21. Gerhard A. Holzapfel, “Nonlinear Solid Mechanics: A Continuum Approach for Engineering,” Book, Wiley Pubs, New York, ISBN: 978-0-471-82319-3 April 2000 470 Pages.
22. ALE3D Computational Manual Material Model, Developed at the Lawrence Livermore National Laboratory
    7000 East Avenue • Livermore, CA 94550.
23. Material properties of S-Glass Fibre, https://www.azom.com/properties.aspx?ArticleID=769
24. Robert M. Jones, “Mechanics of Composite Materials,” Scripta Book Company, Washington D.C. 1975.
25. Weeks, C.A., and C.T. Sun, “Modeling non-linear rate-dependent behavior in fiber-reinforced composites,” **Composites Science and Technology**, **Volume 58, Issues 3–4**, March–April 1998, Pages 603-611
26. Murakami, Sumio, and Yan Liu. "Local approach of fracture based on continuum damage mechanics and the related problems." *Journal of the Society of Materials Science, Japan*45.9Appendix (1996): 131-142.

27. Ljustina, Goran, Martin Fagerström, and Ragnar Larsson. "Rate sensitive continuum damage models and mesh dependence in finite element analyses." *The Scientific World Journal* 2014 (2014).

APPENDIX

Appendix A:

General Simulation information																							
Contact Boundary								*Boundary Conditions*															
AutoContact								roller symmetry y, z															
Elas Model-Fiber Composite Model																							
Density (g/cm^3)		*Ea (MBar)*		*Eb (MBar)*		*Ec (MBar)*		*Poisson ba*		*Poisson ca*		*Poisson cb*		*Gab (MBar)*		*Gbc (MBar)*		*Gca (MBar)*					
1.959		0.22203		0.22203		0.1611		0.4151		0.2057		0.2057		0.049407		0.0463		0.0463					
YS Model- Hyperelastic Progressive Damage Model																							
G	*K*	*Beta*	*Bulk_f*	*kfiber*	*kfiber SR*	*ks*	*ks SR*	*sm*	*sm SR*	*je*	*je SR*	*fiber*	*fiber SR*	*cfiber*	*cfiber SR*	*td*	*td SR*	*sd*	*sd SR*	*ks_d*			
4.63E-02	1.58E-01	-2	N/A	8.69E-03	0.1	3.90E-03	0.1	1.00E-03	0.1	0.4	0.15	4.30E-02	1	5.00E-02	1	4.00E-04	0.1	1.00E-05	0.1	0.1			
YS Model Flags and other parameters																							
Decayparam		*SR opt*		*d_max*		*f_updt*		*dammodel*		*failcpl*		*compfail*											
5		Logarithmic		1		0		0		1		1											

VITA

Nick Scott

EDUCATION

Bachelor of Science (May 2014) in Mechanical Engineering, Southern Methodist University, Dallas, Texas.

ACADEMIC EMPLOYMENT

Graduate Teaching Assistant, Department of Mechanical Engineering, University of Mississippi, August 2017 - present. Responsibilities include: assisting professors with the preparation and presentation of undergraduate courses, grading, and mentoring.

Summer Student Fellow and External Collaborator, Computational Engineering Division, Lawrence Livermore National Laboratory, May 2019-present. Responsibilities include: computational research of high velocity impact on various different experimental setups

Academic Tutor, Southern Methodist University, August 2011-2015. Responsibilities included: tutoring and mentoring undergraduate students of several disciplines, for a multitude of classes in different subjects.